Article

Not peer-reviewed version

Role of Faulting in Salt Deformation and Hydrocarbon Trapping in the Missan Oilfields, Southeastern Iraq

Hayder Yousif , Xuri Huang * , Guanyu Zhang

Posted Date: 1 October 2025

doi: 10.20944/preprints202510.0031.v1

Keywords: Missan oilfields; Zagros Foredeep Fault; salt structures; salt tectonics; fault-controlled reservoirs

Article

Role of Faulting in Salt Deformation and Hydrocarbon Trapping in the Missan Oilfields, Southeastern Iraq

Hayder Yousif [1,2], Xuri Huang [1,*] and Guanyu Zhang [1]

[1] School of Geoscience and Technology, Southwest Petroleum University, Chengdu, Sichuan 610599, China
[2] Geology and Reservoirs Department, Missan Oilfields Operating Authority, Missan Oil Company, Missan 62001, Iraq
* Correspondence: 190466848@qq.com

Abstract

We investigate the relationship between faulting, salt deformation, and hydrocarbon accumulation in the Missan oilfields, southeastern Iraq, by integrating seismic, well, and surface data. The analysis reveals a clear correlation between surface topographic highs and subsurface salt-related deformation, which aligns with broader deformation trends observed along the Zagros Fold–Thrust Belt (ZFTB). The Buzurgan field showed limited evidence of fault reactivation, with consistent folding persisting until the Late Miocene, while the Fauqi and Abu Ghirab fields experienced Pliocene reactivation and intense salt deformation, resulting in structural disharmony characterized by syncline-over-anticline geometries. Closely spaced faults enhanced salt deformation, forming complex listric and conjugate fault systems aligned with basement-related faults, confirming their mechanical linkage. Fault activity critically influenced hydrocarbon migration: intense faulting in Abu Ghirab enabled vertical leakage to shallow reservoirs (Kirkuk Formation), while minimal fault activity in Buzurgan restricted hydrocarbon accumulation to deeper layers (Mishrif Formation), and moderate fault activity in Fauqi allowed entrapment in both the Mishrif and Kirkuk reservoirs. These findings highlight the crucial role of fault–salt interactions in controlling reservoir heterogeneity and hydrocarbon distribution, offering valuable insights for exploration in structurally complex settings.

Keywords: Missan oilfields; Zagros Foredeep Fault; salt structures; salt tectonics; fault-controlled reservoirs

---

1. Introduction

Faulting plays a critical role in tectonic and hydrocarbon systems, influencing salt deformation and reservoir dynamics [1–6]. In many compressional settings, particularly within foreland basins like the Zagros Fold–Thrust Belt (ZFTB), the interplay between deep-seated basement faults and overlying evaporite sequences governs both the geometry of structural traps and the effectiveness of sealing formations. Numerous studies in southwestern Iran have explored this dynamic, revealing how salt bodies behave under regional stress regimes and how their deformation relates to tectonic shortening and sedimentary loading [7–23]. These investigations address critical questions, such as when and why salt penetrates overlying layers, and whether a direct relationship exists between salt deformation and regional folding.

Salt-related studies remain ongoing, considering the necessity of penetrating salt-bearing layers to access oil reserves and the availability of extensive seismic and drilling data. Western Iran and southeastern Iraq represent a region where faulting and salt tectonics have significantly influenced the formation of hydrocarbon reservoirs. Despite several studies on hydrocarbon accumulation and

 doi:10.20944/preprints202510.0031.v1

petrophysical properties in southeastern Iraq [24–28], the role of faulting in facilitating or impeding hydrocarbon migration in the Missan oilfields remains insufficiently addressed.

Salt deformation is fundamental to the tectonic evolution of sedimentary basins and exerts a critical influence on hydrocarbon distribution [29]. In provinces with thick evaporite accumulations, such as the ZFTB, salt-related structures—including diapirs, pillows, and welds —respond not only to regional stresses but also actively influence the localization, geometry, and kinematics of fault systems. Conversely, basement-involved and strike-slip faulting can trigger salt mobilization and welding, producing rotated, segmented, and prematurely terminated faults—a reciprocal interaction documented across the ZFTB [11,30]. Understanding these bidirectional fault–salt interactions in the Missan oilfields is therefore essential for optimizing exploration and production strategies in salt-influenced foreland settings. To that end, this study builds a geomechanical model of fault–salt interaction by integrating 3D seismic, well logs from >300 wells, and seismic-attribute analysis, with objectives to: (1) classify fault types and quantify their spatial relationships to salt bodies; (2) evaluate how structural reactivation modulates deformation intensity across the Missan fields; and (3) interpret the implications for hydrocarbon migration and entrapment.

1.1. Regional Tectonic Evolution of the Arabian Plate

The Arabian Plate underwent rifting from the Late Permian to the Early Triassic, leading to the formation of the Neo-Tethys Ocean [31–33]. This rifting phase was followed by the development of a passive margin and post-rift thermal subsidence during the Jurassic to Late Cretaceous [31]. Nonetheless, multiple lines of evidence indicate renewed Cretaceous extension along segments of the future ZFTB, expressed by syn-depositional normal faulting, horst–graben architecture, and local back-arc opening on the northeastern Arabian margin [34,35]. This tectonic evolution is instrumental in forming some of the Middle East's most significant oil-generating source rocks and hydrocarbon-bearing reservoirs [36]. In the Late Cretaceous, convergence between the Arabian Plate and the Neo-Tethyan oceanic lithosphere began, initiating obduction and inversion along the northeastern margin of the Arabian Plate [37]. The Neo-Tethys then closed diachronously, with final suturing from the Late Oligocene to early–middle Miocene, bringing Arabia into direct contact with Eurasia [31]. Collision drove crustal shortening, regional uplift, and foreland deposition; in the Mesopotamian foreland, thick Miocene clastic–evaporite successions (Fatha) accumulated in restricted-marine to lagoon–sabkha settings [38], and earlier salt layers were then buried to depths exceeding 2000 m in the study area [39], with local well data indicating burial to ~2800 m. This broader tectonic context, including plate convergence, foreland basin development, and syn-tectonic sedimentation, provides the framework for understanding the structural evolution of the Missan oilfields. Figure 1 illustrates the Middle Miocene depositional setting and the position of the study area in southeastern Iraq, where the Zagros Foredeep Fault (ZFF) intersects the region.

Preprints.org (www.preprints.org) | NOT PEER-REVIEWED | Posted: 1 October 2025 doi:10.20944/preprints202510.0031.v1

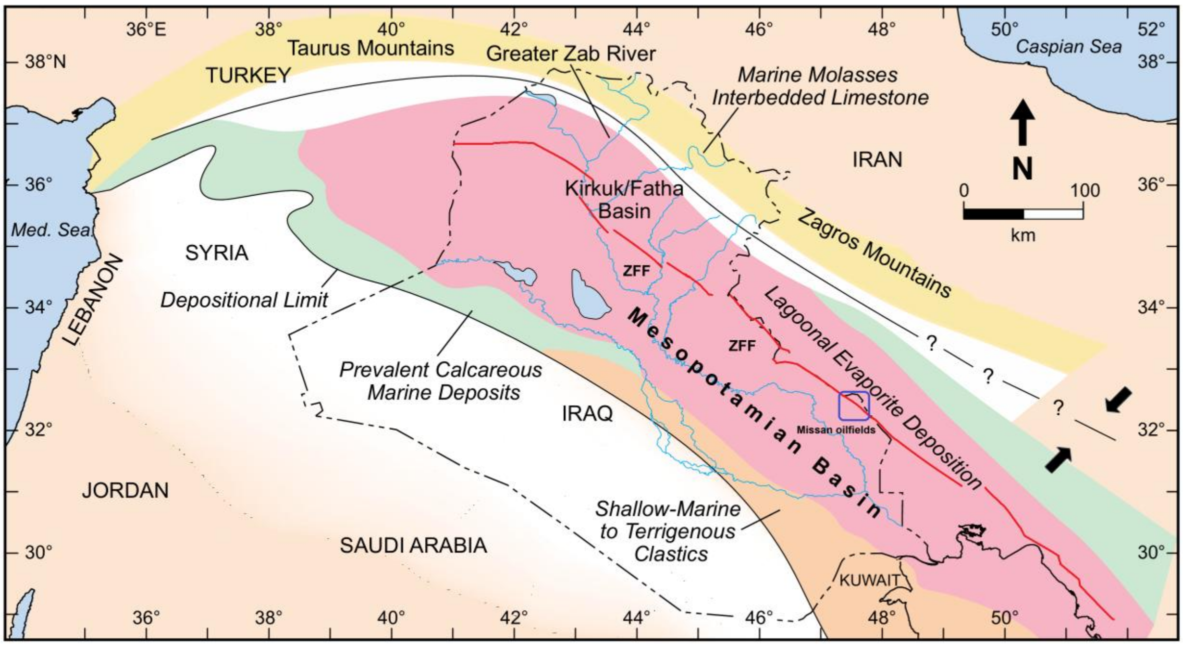

Figure 1. Regional paleogeographic map illustrating the depositional setting of the Middle Miocene Fatha Formation across the Mesopotamian Basin. The pink-shaded area indicates lagoonal evaporitic deposition. Key structural features, including the Zagros Mountains and major depositional environments, are illustrated. The study area is marked with a blue box in southeastern Iraq, where the ZFF also passes through. The base map was modified from [38], with the location of the ZFF added in accordance with [40].

In Iran, the ZFTB is divided into the Fars, Izeh, and Lurestan zones, separated by major oblique transfer zones. Two regional embayments, the Dezful Saddle in Iran and the Kirkuk Saddle in Iraq, form structural lows known as syntaxes [19,41,42]). These embayments are younger than the Upper Oligocene to Lower Miocene Kirkuk Formation and represent ongoing subsiding sedimentary basins from the Middle Miocene, characterized by terrigenous and shallow-marine siliciclastic deposits that reflect syn-tectonic sedimentation [44].

The Buzurgan, Fauqi, and Abu Ghirab oilfields, collectively referred to as the Missan oilfields, are situated in southeastern Iraq, with parts of Fauqi and Abu Ghirab extending across the border into Iran (Figure 2). These fields lie within the Dezful Embayment [22,39,44,45], specifically in the foothills subzone along the margin of the Mesopotamian Zone.

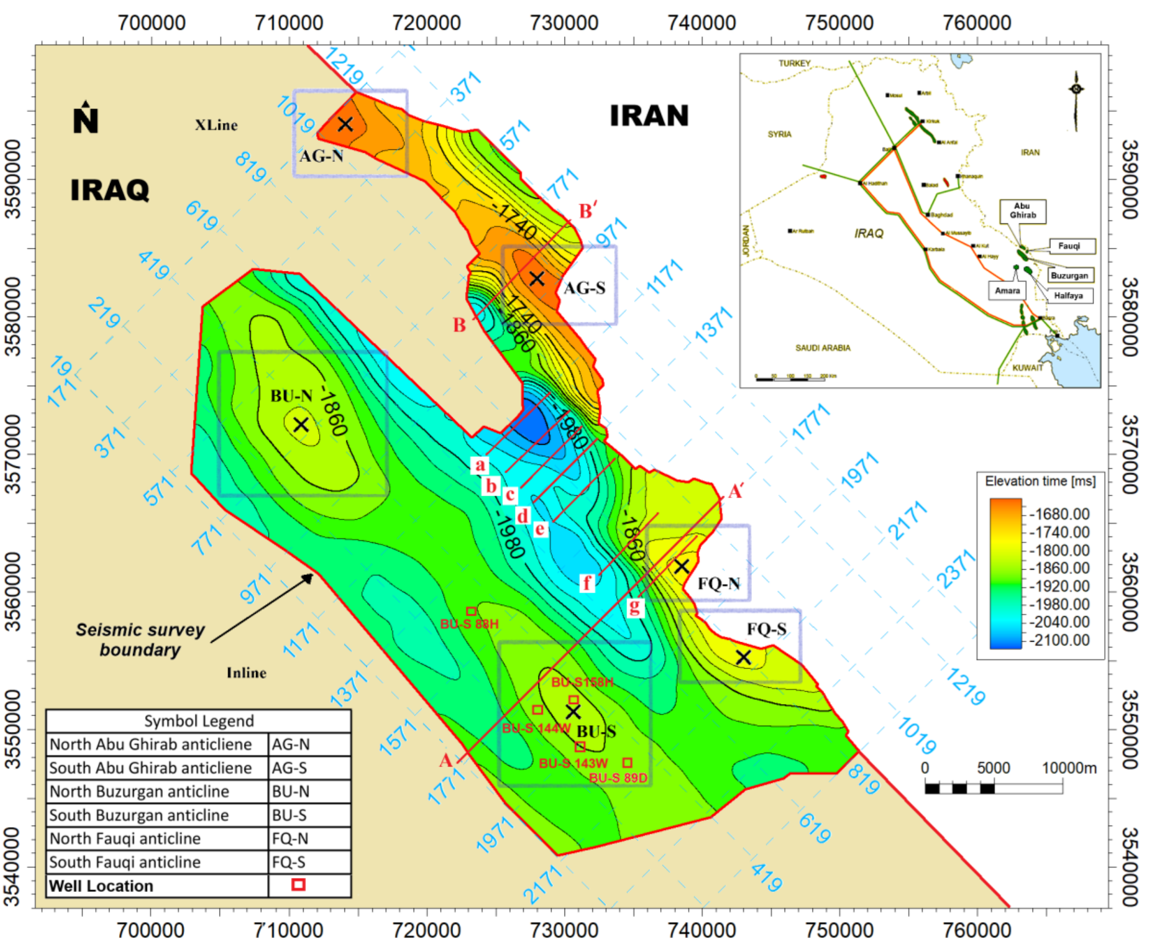

Figure 2. Time-structural map of the top MB1 horizon within the Fatha Formation, representing the base of the Mobile Group. The map illustrates the structural configuration and spatial distribution of the Missan oilfields, specifically Abu Ghirab, Buzurgan, and Fauqi, within the boundary of the interpreted 3D seismic survey. Color contours indicate structural depth in milliseconds (two-way travel time), with warmer colors corresponding to shallower intervals. The inset map shows the locations of the Missan oilfields in southern Iraq.

Structurally, the region is more complex than the adjacent Mesopotamian Zone, which lacks prominent surface folding [46]. It is characterized by narrow, asymmetrical anticlines often detached along Middle Miocene evaporite layers. These evaporites not only localize fault detachment surfaces but also influence the geometry of folds. In many cases, core zones of major anticlines expose younger clastic deposits due to erosion or late uplift [46].

1.2. Salt Tectonics in the Fatha Formation

The Fatha Formation (previously referred to as the Lower Fars Formation) primarily comprises evaporite rocks, such as anhydrite, marl, and locally halite, deposited in extensive lagoons and embayments during repeated marine incursions [47]. It evolved into a broad, shallow foreland basin in front of the emergent Zagros Mountain chains [9]. Despite its wide extent, significant salt accumulations in Iraq are limited to the Kirkuk Embayment in the north [38] and the Missan region in the south as part of the Dezful Embayment [48]. Salt deformation is most pronounced close to the Zagros Fold–Thrust Belt and diminishes southwestward into the foreland basin. Accordingly, salt layers in fields such as Amara and Halfaya appear relatively undeformed due to their greater distance from the ZFTB and the ZF (Figures 2 and 6). In contrast, the salt in the present study area shows significant deformation, reflecting its proximity to these tectonic structures.

Salt deformation is primarily driven by variations in overburden weight and compressional forces associated with continental collision [8,49,50], causing salt to migrate from high-pressure to low-pressure zones. This deformation is more pronounced in areas closer to the Arabian–Eurasian collision zone, such as southwestern Iran. It becomes progressively less intense toward the tectonic margin in southeastern Iraq. This spatial trend indicates that the degree of salt deformation diminishes southwestward from the ZFTB, suggesting that deformation intensity decreases with increasing distance from the belt, regardless of the nature of the driving forces.

The occurrence of salt within structurally deformed zones exerts a pronounced influence on subsurface conditions by redistributing stress across mechanically weaker layers [51]. In the Missan region, the thick evaporitic successions of the Fatha Formation play a particularly critical role, as they govern both the style of deformation and the development of associated pressure anomalies. Consequently, salt not only represents a mechanically distinctive unit within the stratigraphic succession but also constitutes a key factor shaping the broader geomechanical framework of the study area. The operational implications of this relationship are discussed in detail later in this paper.

1.3. Stratigraphy and Regional Significance of the Fatha Formation

The Fatha Formation, a key unit of the Middle Miocene, has been extensively debated regarding its age. Studies have proposed ages ranging from Lower to Middle Miocene, a strictly Middle Miocene age [52], a Lower Miocene age [53], and a diachronous age [47]. The formation was originally described in Iran by Busk and Mayo in 1918 [52]. In Iranian literature, it is now formally referred to as the Gachsaran Formation [54]. The Fatha Formation extends across Syria, Iraq, and Iran [9] which underscores its stratigraphic and tectonic significance across the region. It plays a crucial role as a cap rock for many oil reservoirs in eastern Iraq and western Iran due to its composition of low-permeability evaporites such as anhydrite and halite, along with shale, which effectively inhibits hydrocarbon migration [48,55–57].

The formation is subdivided into distinct units across different regions. In Iran, it comprises seven formal units [54], while in northern Iraq, it is classified into three units [52]. Five informal subdivisions were identified by early oil exploration geologists in southeastern Iraq, from top to bottom, these are: MB5, consisting of alternating beds of anhydrite and shale; MB4, composed of interlayered anhydrite, shale, and salt; MB3, a thick anhydrite unit interbedded with salt, shale, and occasional limestone; MB2, characterized by massive salt deposits; and MB1, primarily composed of anhydrite with thin interbeds of shale and shaly dolomite (see Table 1).

doi:10.20944/preprints202510.0031.v1

Table 1. Stratigraphic column of the Buzurgan oilfield, including geologic age, formation tops, pressure coefficients, drilling risks, lithological descriptions, tectonic mega-sequences [31], and mechanical competency classification [8]. Pressure and lithological data are based on well data from the study area.

Age		Strata		Top Depth (TVDss)	Pressure coefficient	Drilling risks	Lithology description	Competency	Tectonic Mega Sequence (TMS)
Quaternary		Bai Hassan-Mukdadiya		——	——	Bit balling	Clay, Gravel and Sand	Incompetent Group	Zagros orogeny (AP11)
Tertiary	Upper	Injana (Upper Fars)		≈ -600	about 1.04	Caving & bit balling	Mainly Clay(upper), Mainly Shale interbed with Sand		
	Middle Miocene	Fatha (Lower Fars)	(Mb5)	-2074.5	Transition zone	Natural flow	Alternation of anhydrite, Shale		
			(Mb4)	-2379.5	2.20~2.22	Super pressure and gas cut	Alternation of anhydrite, Shale and Salt	Mobile Group	
			(Mb3)	-2648.5	2.20~2.22	Super pressure and gas cut	Thick bed of anhydrite interbedded with salt and shale with rare limestone		
			(Mb2)	-2789.5	2.20~2.22	Super pressure and gas cut	Massive salt		
			(Mb1)	-2793.5	Transition zone	Loss	Anhydrite with thin inercalation of shale and shaly dolomite	Competent Group	
	Lower Miocene	Jeribe-Euphrate		-2821.5	1.1	Loss	Massive dolomite , locally limestone and anhydritic interbeded with reddish brown shale		
		Upper Kirkuk		-2876.5	1.1	Loss	Mainly dolomite interbedded with sandstone, limestone, and mudstone		Closure of Neo-Tethys (AP10)
	Oligo - cene	Middle-Lower Kirkuk		-2990.5	1.1	Loss	Sandstone and shale		
	Paleocene-Eocene	Jaddala		-3205.87	1.1	Loss	Argillaceous Limestone, Marl, Shale, and Chert		
		Aaliji		-3336.69	1.1	Gas cut	Limestone		Active northeast margine (Ophiolite obduction) (Ap9)
Cretaceous	Upper Cretaceous	Shiranish		-3380.36	1.1	Hole shrinkage	Argillaceous Limestone		
		Hartha		-3401.53	1.1	Loss & Sloughing shale & gas cut	Chalky and argillaceous Limestone		
		Sadi		-3471.81	1.1	Gas cut & Sloughing shale	Argillaceous limestone and marl with thin shale		
		Tanuma		-3609.7	1.1	Sloughing shale	Shale, limestone with marl		
		Khasib		-3627.68	1.1	Sloughing shale& Loss & Gas cut	Compact limestone		Post rift passive margine of Neo-Tethys ocean opening (AP8)
		Mishrif	MA	-3692.46	1.1	Loss	Compact limestone		
			MB11	-3793.4	1.1	Loss	Compact limestone interbedded with thin packstone		
			Mb12	-3802.8	1.1	Loss	Compact limestone interbedded with thin packstone		
			MB21	-3834.81	0.91	Loss	Mainly grainstone		
			MB22	-3890.55	1.12		Limestone		
			MC11	-3958.19	1.12		Limestone		
			MC12	-3990.98	1.12		Limestone		
			MC2	-4026.94	1.12		Limestone		
TD				-4117.8					

2. Materials and Methods

We conducted a series of analyses to investigate salt deformation and fault interactions in the Missan oilfields:

A 3D post-stack time-migrated seismic dataset covering ~113 km² across the Missan oilfields in southeastern Iraq was employed (Figure 2). The dataset, provided by the Iraqi Oil Exploration Company (OEC), has a 2 ms vertical sampling interval, 25 × 25 m bin size, and a dominant frequency of 28–30 Hz, yielding moderate vertical resolution suitable for horizon and fault delineation. Seismic interpretation was conducted in Schlumberger Petrel, and detailed mapping of structural and stratigraphic elements was achieved.

Two NE-SW-trending seismic lines were chosen to cross the Abu Ghirab, Fauqi, and Buzurgan anticlines (Figures 5 and 11), allowing for a structural analysis of fold geometries. Additionally, seven parallel seismic cross-sections were taken along the southeastern limb of the Fauqi Fold (Figure 9) to examine the spatial distribution and geometry of salt-related deformation in relation to underlying deep-seated faults.

A comparative analysis was conducted between the present-day surface topography and subsurface deformation patterns associated with salt structures. This assessment, utilizing satellite imagery and elevation profiles derived from Google Earth (Figure 8), provided corroborative evidence linking surface morphological expressions to underlying salt-related deformation and associated deep-rooted faults.

More than 300 wells were analyzed using sonic and gamma-ray logs, complemented by density and velocity logs where available. From this extensive dataset, five representative wells located in the southern dome of the Buzurgan field, reaching depths of approximately 3700 meters, were selected for detailed lithological assessment (Figure 3). These wells facilitated the characterization of lithofacies variations within the Fatha Formation, specifically targeting interbedded salt, shale, and anhydrite intervals of the Mobile Group. The salt-bearing intervals within this group occur predominantly at depths ranging from approximately 2350 to 2800 m. Additionally, synthetic seismograms were constructed to accurately tie seismic reflections to well-log data, thereby improving the precision of horizon correlations.

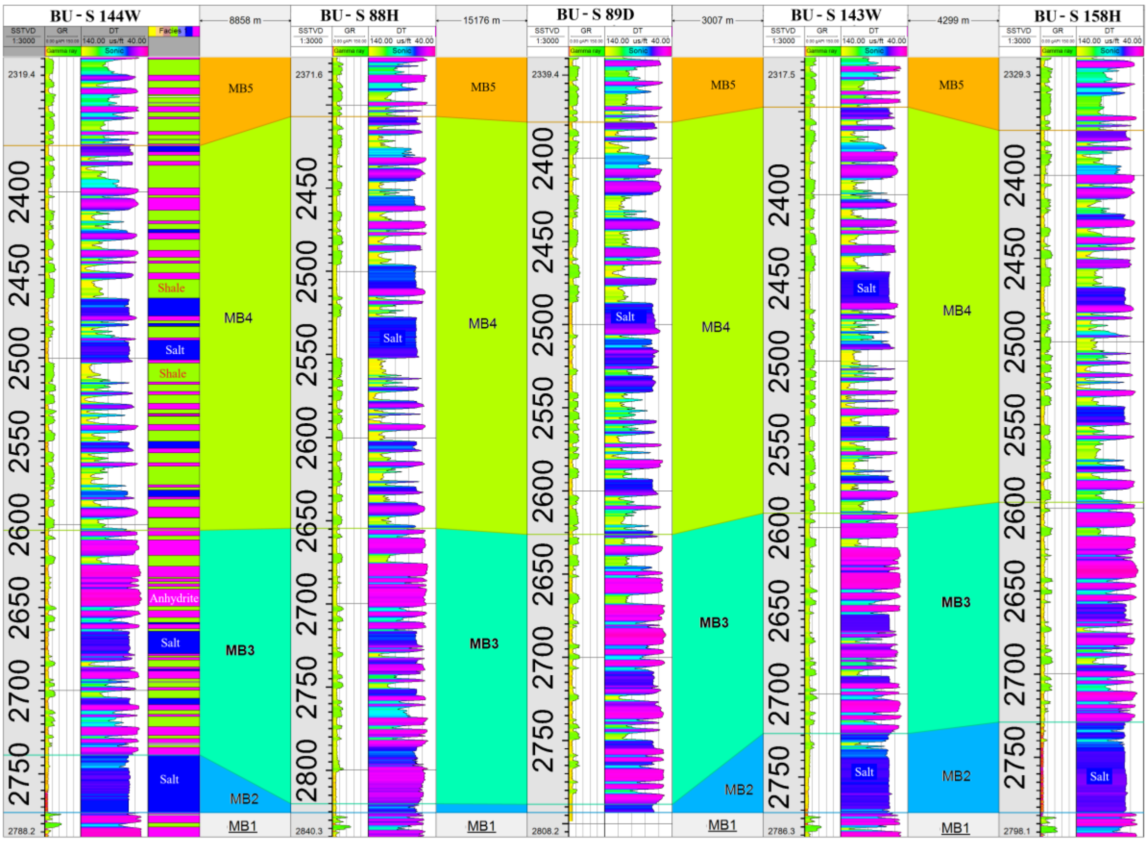

Figure 3. Cross-section showing sonic and gamma-ray logs from five wells in the Buzurgan oilfield, illustrating significant variations in salt bed thickness, particularly in unit MB2. The pinch-and-swell geometry reflects structural deformation caused by the mobility of salt.

To establish the broader structural context, a regional tectonic framework was constructed using seismic inline 1748, integrated with structural trends and geological data from adjacent oilfields. This integration aimed to link present-day subsurface geometries with the region's tectonic evolution and to constrain the timing and mechanisms of salt mobilization and fault reactivation.

To support the identification of deep-rooted compressional structures, regional fault data were incorporated from both published seismological sources and the tectonic map of Iraq. This national map, developed using 2D seismic interpretation, highlights the presence of reverse and thrust faults

Preprints.org (www.preprints.org) | NOT PEER-REVIEWED | Posted: 1 October 2025 doi:10.20944/preprints202510.0031.v1

that traverse the study area. These features were used to guide and constrain the structural interpretation of the 3D seismic volume. To further enhance the visualization of fault geometries and stratigraphic discontinuities—particularly within the Jaddala Formation—a variance attribute was applied using a trace-to-trace similarity algorithm (Figure 7). The resulting attribute volume was compared with depth-structure maps (Figure 6) to verify fault continuity and increase confidence in the interpreted structural framework.

3. Results

3.1. Thickness Variations of the Mobile Group in the Missan Oilfields

The sonic log measures the travel time (Δt) of acoustic waves as they propagate through geological formations in boreholes, providing essential insights into lithological characteristics [58]. Reliable lithological differentiation of evaporitic sequences—even those comprising thin interbeds—can be achieved using a combination of sonic and gamma-ray logs. Laboratory measurements and borehole data confirm that sonic values for pure halite typically range between 67 and 69 μs/ft. In contrast, anhydrite exhibits lower sonic values due to its higher density and rigidity, which allow faster acoustic wave transmission. Shale, despite its comparable density, exhibits higher sonic readings due to its greater porosity and produces elevated gamma-ray responses resulting from its enriched radioactive mineral content. Figure 3 displays sonic and gamma-ray logs from five representative wells in the southern Buzurgan oilfield, illustrating clear differences in MB2 thickness, an interval composed entirely of salt.

Across the broader Missan region, the Mobile Group (MB2) displays distinct spatial patterns in thickness. In the Halfaya and Amara fields, south and southwest of the study area (Figure 2), MB2 is relatively uniform at ~20 m. By contrast, substantial variability occurs in the Buzurgan, Fauqi, and Abu Ghirab fields, where thicknesses range from only a few meters to more than 70 m. Figure 4 presents a time-thickness (isochron) map of the Mobile Group (MB4–MB2), illustrating pronounced lateral heterogeneity across the study area. These thickness variations provide the basis for interpreting the structural controls that influence salt deformation.

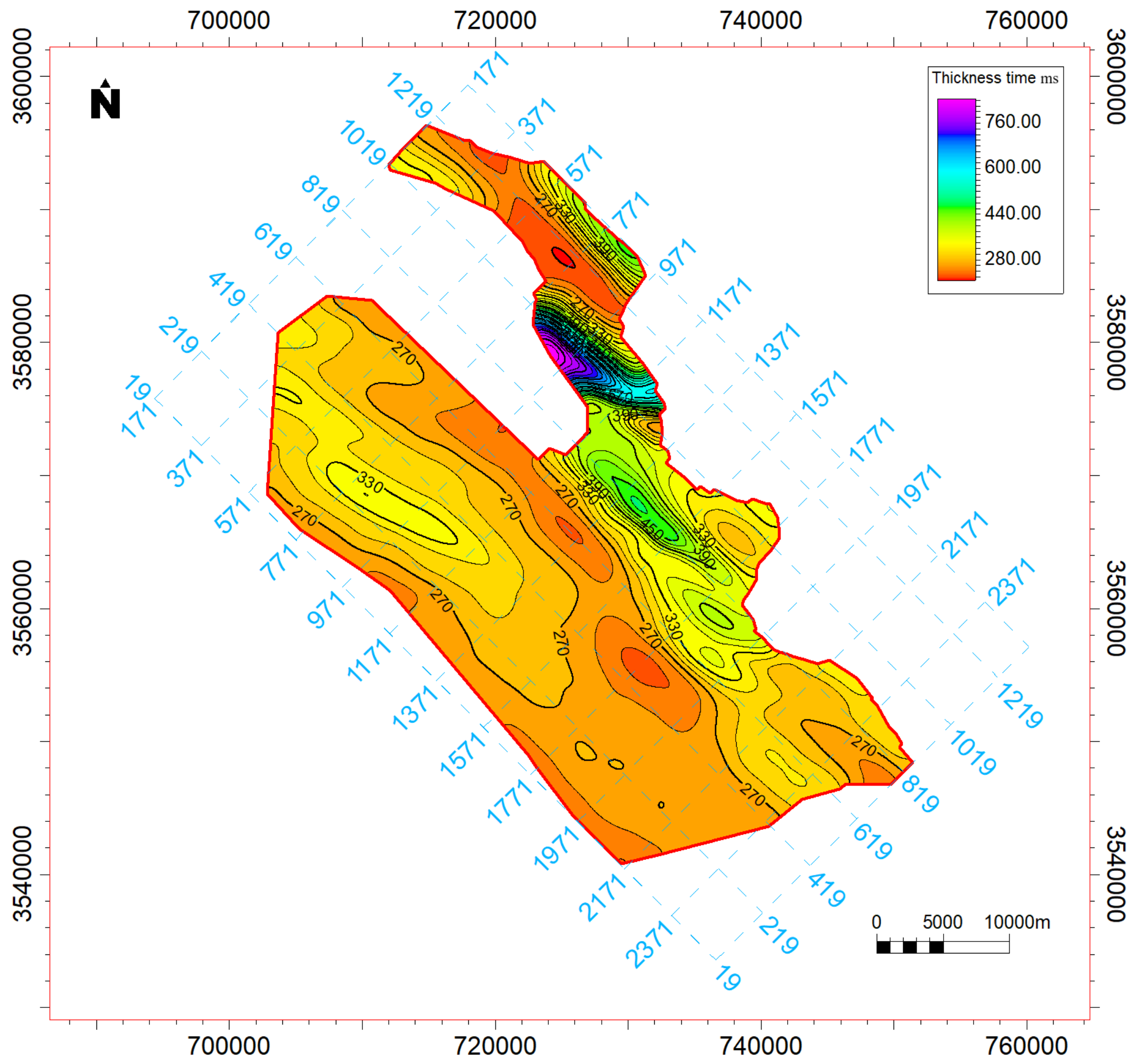

Figure 4. Isochron (time-thickness) map of the Mobile Group (MB4–MB2) across the Missan oilfields, illustrating spatial variations in interval thickness. Fault locations are shown for reference in Figure 6.

3.2. Stratigraphic and Tectonic Interpretation

The interpreted seismic section crossing the Buzurgan and Fauqi anticlines (Figure 5) shows a transition from continuous, parallel reflectors in deeper intervals to discontinuous and chaotic reflectors in shallower levels. In the deeper section, reflectors are continuous and parallel, representing mechanically competent carbonate strata that are predominantly composed of limestone. Upward, seismic reflectors become increasingly discontinuous and chaotic, especially near the core of the Fauqi anticline.

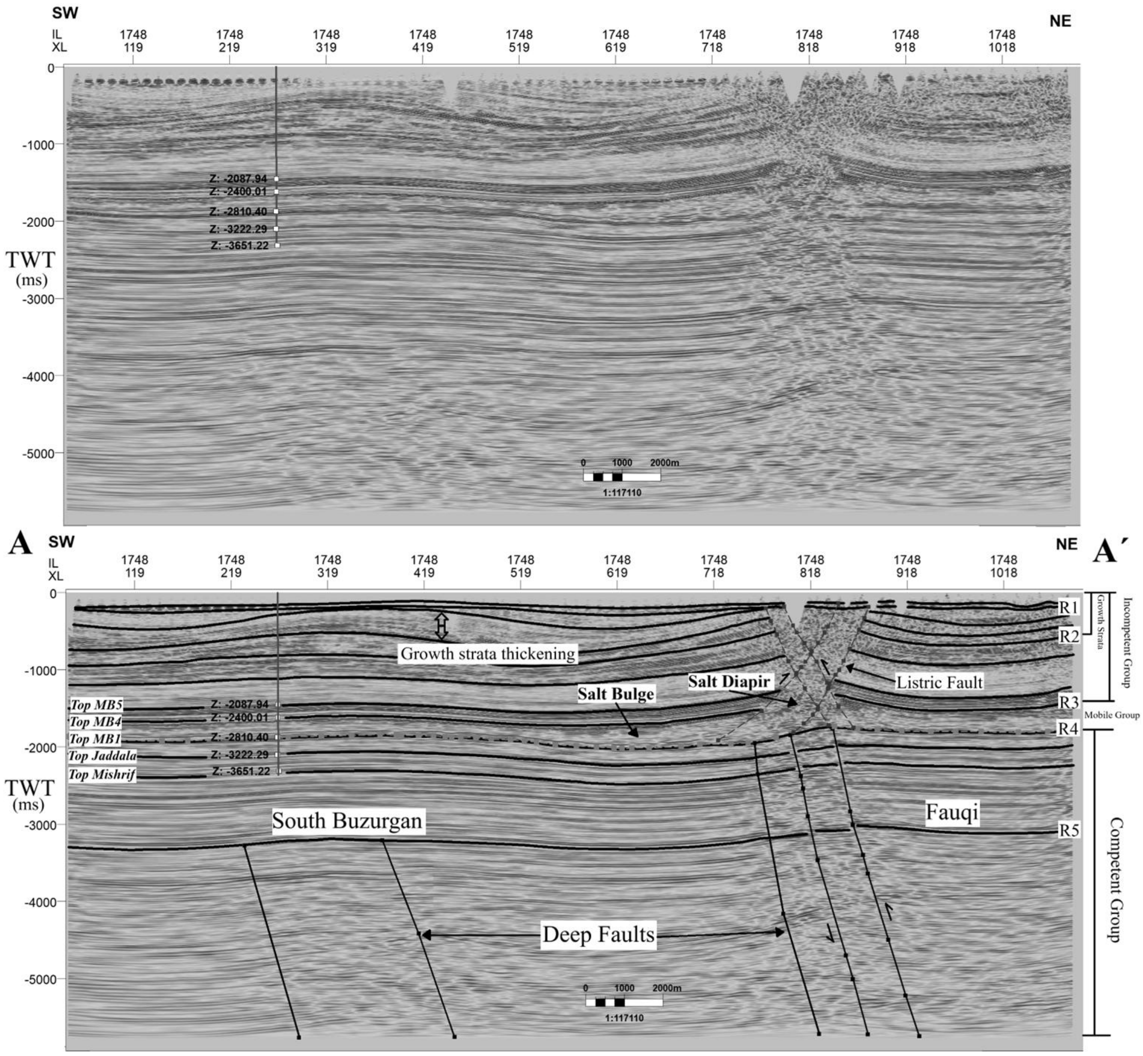

Figure 5. Seismic section A-A′ across the South Buzurgan and Fauqi structures. The upper panel shows the uninterpreted post-stack time-migrated section (inline 1748), while the lower panel presents the interpreted version. Key structural features include deep-seated reverse faults, a salt bulge, a salt diapir, and listric faulting above the Mobile Group. Stratigraphic horizons and mechanical stratigraphy (Competent, Mobile, and Incompetent Groups) are also highlighted. The reflectors R1 to R5 represent key seismic horizons used for interpretation and analysis. The location of this seismic section is shown in Figure 2.

Five primary reflectors (R1–R5) are identified: R1 is a shallow near-surface reflector closely following surface topography; R2 marks the base of the growth strata, above which thickness variations indicate syn-depositional accumulation during folding; R3 defines the top of MB4, characterized by a pronounced salt-related structural uplift; R4 delineates the base of the Mobile Group, equivalent to the top of MB1 within the Fatha Formation, indicating the lower boundary of salt influence; and R5 corresponds to a deep reflector marking the top of a rift-influenced interval, likely of Triassic age.

Following [7,8], we adopt a simplified tripartite scheme tailored to the Missan sector: the Incompetent Group (Late Miocene–Quaternary clastics), the Mobile Group (Middle Miocene Fatha evaporites), and the Competent Group (pre-Miocene carbonates). In practice, the available seismic profiles image only these three divisions; O'Brien's deeper units—the Basement and the Lower Mobile Group (Ediacaran–Cambrian Hormuz Salt)—lie below the imaged interval and are not observed in this dataset. The reflector–unit relationships are: R1–R2 within the Incompetent Group (with R2 marking the base of growth strata), R3–R4 bounding the Mobile Group (Fatha evaporites), and R5 lying within the Competent Group and marking the top of the rift-influenced interval.

 doi:10.20944/preprints202510.0031.v1

3.3. Structural, Faults, and Salt Deformation Interpretation

The NE–SW seismic section along inline 1748 (Figure 5) images the subsurface beneath the Buzurgan and Fauqi structures and reveals two prominent anticlines. Within the inter-anticline syncline of the Mobile Group, a salt pillow (bulge) develops, where the salt thickens but does not breach the overburden. In contrast, a discrete salt diapir pierces the cover along the left limb of the Fauqi fold. Three fault families are distinguished in the Missan oilfields based on geometry, stratigraphic extent, and relationship to salt flow: (i) steep, basement-involved deep-seated faults; (ii) bedding-parallel detachment faults developed within the evaporitic units of the Fatha Formation (Mobile Group); and (iii) listric growth faults that sole into the detachment and propagate upward into the overlying strata. To better clarify the structural framework, these three fault families are grouped and described in terms of their kinematic characteristics and petroleum significance (Table 2).

Table 2. Classification of fault types in the Missan oilfields.

Fault Group	Characteristics	Stratigraphic Level	Kinematics / Geometry	Observed Role
Deep-Seated Basement Faults	High-angle faults rooted in the basement; some extend upward into the mobile group, others terminate in Triassic–Jurassic strata.	Basement to Triassic–Jurassic to Fatha Formation.	Reactivated from normal to reverse during Pliocene compression.	Controlled regional folding and provided vertical migration pathways.
Detachment (Décollement) Faults	Low-angle, regionally extensive detachments within the Mobile Group (salt/shale/anhydrite).	Primarily along R4 (major) and locally along R2 (minor).	Acted as mechanical decoupling surfaces, accommodating significant shortening; facilitated disharmonic folding above salt.	Produced syncline-over-anticline geometries and localized listric/conjugate fault systems.
Listric Faults	Inclined, curved geometries; often conjugate sets; flatten into décollement at depth.	Propagate through the Mobile Group into overlying formations (Fatha–Injana).	Developed under the combined influence of horizontal compression and salt uplift.	Enhanced salt mobilization

1. Deep-seated faults are expressed as steep to near-vertical structures indicative of basement-involved deformation and reverse (thrust) kinematics. In the Dezful Embayment, where Hormuz salt is absent, the basal décollement is interpreted within Lower Paleozoic shales [10] consistent with a basement origin for these thrusts. Their upper tip lines are sharp and represent the steep, near-surface segments of thrusts captured by the seismic section; in compressional settings, such shallow segments commonly steepen due to folding and fault propagation, whereas at depth, the same faults are expected to flatten onto a low-angle décollement that lies below or outside the imaged window. Termination depths vary—some fault tips terminate at the base of the Fatha base (Figure 5; Fauqi fold), where salt accommodated shortening, whereas others root deeper, likely within Triassic units

Preprints.org (www.preprints.org) | NOT PEER-REVIEWED | Posted: 1 October 2025 doi:10.20944/preprints202510.0031.v1

(Figure 5; Buzurgan fold). Diapiric salt flow absorbed a significant fraction of orogenic stress and focused thrust nucleation and growth, thereby exerting a first-order control on fault development [11].

Some deep faults were activated by the collision between the Arabian and Eurasian plates, which resulted in the formation of the ZFF fault. This fault delineates the boundary between the folded and the Mesopotamian zones [46]. The spatial configuration of these deep-seated faults, as interpreted from seismic data, corresponds closely to the regional structural framework. This relationship is illustrated in Figure 6, where: (a) presents a regional tectonic map of Iraq showing the main tectonic zones and fault systems, with the study area in southeastern Iraq highlighted for reference (modified after [59]), and (b) displays the time-structure map of the Jaddala Formation within the Missan oilfields, highlighting the alignment of deep-seated faults with the fault traces mapped at the regional scale. Notably, in the Buzurgan area, such deep-seated faults are absent from the map in (b) because they terminate at considerable depth, below the imaged interval.

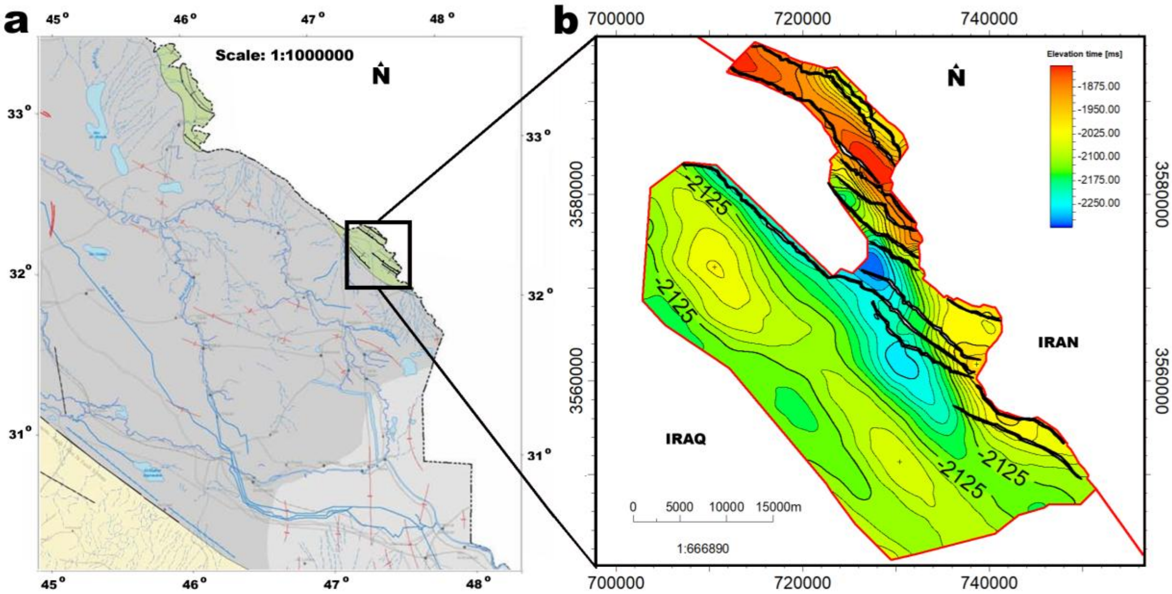

Figure 6. (a) Regional tectonic map of Iraq depicting the major tectonic zones and fault systems, with the study area in southeastern Iraq delineated for reference (modified after [59]) (b) Time-structure map of the Jaddala Formation within the Missan oilfields, highlighting the configuration of deep-seated faults that spatially correspond to the fault traces observed in the regional framework shown in (a).

The variance attribute is applied to the seismic volume to enhance fault visibility and validate the structural interpretation (Figure 7). This analysis reveals distinct lateral amplitude variations along the Jaddala Formation surface, enabling the delineation of the horizontal extent and distribution of faulting and fracturing. In the Abu Ghirab area, prominent zones of intense faulting are identified, characterized by abrupt amplitude terminations and elevated variance values, indicative of significant structural disruption. By contrast, the Fauqi area exhibits moderate fault development. In contrast, the Buzurgan area shows continuous amplitude patterns and low variance values, suggesting limited fault activity and a more structurally uniform setting.

 doi:10.20944/preprints202510.0031.v1

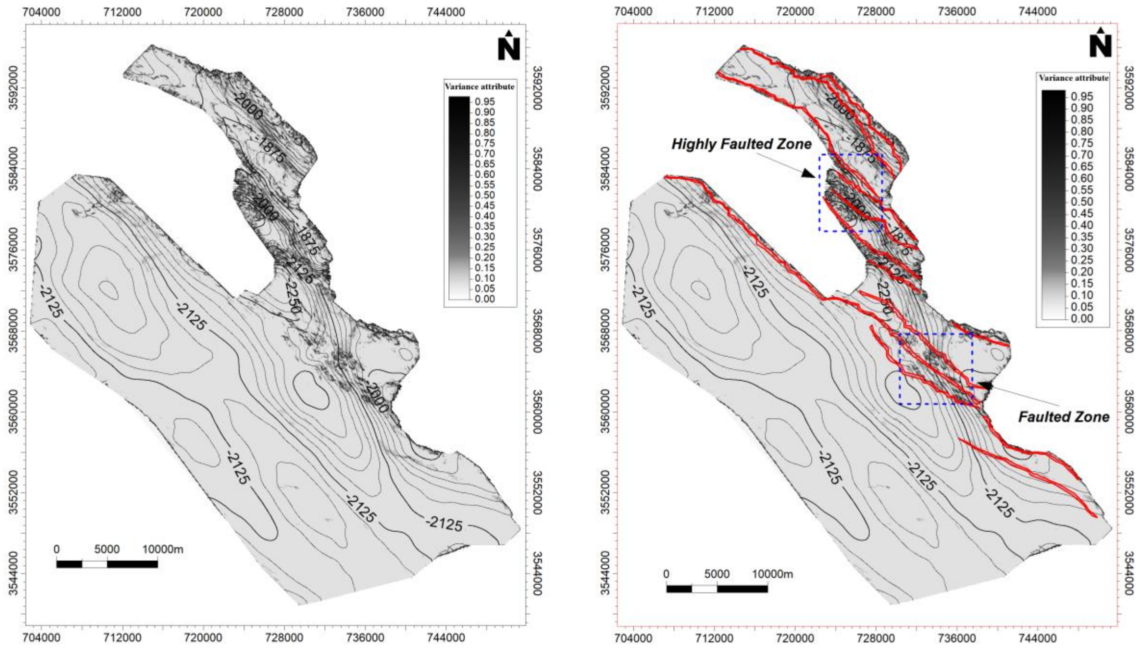

Figure 7. Variance horizon slice of the Jaddala Formation illustrating (a) amplitude variability and (b) interpreted fault patterns (red lines) from seismic data, revealing a strong spatial correlation between variance anomalies and fault structures.

2. Detachment faults formed within the evaporitic layers of the Fatha Formation, where salt served as a mechanical detachment zone in compressional regimes [60]. Numerous studies have identified these faults and regarded the Fatha as the upper main detachment surface [8,10,21,61–65]. Though not clearly visible in seismic sections due to their bedding-parallel nature, they were inferred from thickness variations within the Fatha, especially in salt-rich members MB4, MB3, and MB2 (Figures 3, 5, 9 and 11).
3. Listric faults and low-relief salt structures dominate thin-evaporite regions [60]. Conjugate listric thrust faults are documented in compressional fold-and-thrust settings [66–68] where horizontal shortening promotes the development of oppositely dipping, curved fault planes above a décollement. These faults are typical of folded belts under stable vergence conditions [69], commonly flatten at depth due to horizontal movement above the décollement surface [70].

4. Discussion

Section 3.1 and Figure 4 demonstrate that MB2 thickness varies significantly across the Missan oilfields. The greatest heterogeneity occurs in the Fauqi and Abu Ghirab fields, where proximity to basement-involved faults enhanced salt deformation, whereas the Halfaya and Amara fields display relatively uniform thicknesses. This spatial distribution is consistent with tectonic loading and halokinesis exerting first-order control on salt thickness. Section 3.2 and Figure 5 show a transition from continuous, parallel reflectors in deeper carbonate strata to discontinuous and chaotic reflections near the anticline cores. This reflector geometry is consistent with the presence of evaporitic detachments that decoupled competent and incompetent units, generating disharmonic folding and localized thickening of growth strata during shortening.

In the Buzurgan field, salt deformation is limited because deep-seated faults were either not reactivated or experienced insufficient displacement to trigger salt swelling. The cover strata above the Mobile Group exhibit disharmonic folding, including local syncline-over-anticline geometries consistent with pinch-and-swell thickening of the underlying salt. Figure interpretations further show that shortening and folding are more pronounced in the upper two groups than in the deeper Competent Group, reflecting contrasts in compaction and lithological strength. The Competent

Group, composed primarily of limestone, is more consolidated and mechanically robust than the overlying formations. Growth strata in Buzurgan are largely controlled by fold-related subsidence rather than direct faulting, with thicker packages along the eastern limb indicating asymmetric deformation during progressive shortening. By contrast, in the Fauqi and Abu Ghirab fields, listric faulting combined with salt swelling created additional accommodation space, directly controlling stratigraphic thickening and producing disharmonic geometries. The most diagnostic expression is the development of synclines overlying anticlines, which highlights the combined influence of listric faulting, halokinesis, and upper-stratigraphic deformation.

The variance attribute (Figure 7) highlights a strong spatial correspondence between high-variance anomalies and the fault traces interpreted from the time-structure map (Figure 6). This agreement supports the effectiveness of the variance attribute for fault detection and reinforces the reliability of the mapped fault geometries across the study area.

In the mechanically weak Mobile Group, listric faults developed under folding stresses associated with the Arabia–Eurasia collision. This deformation produced enhanced shortening along the basal décollement compared to the deeper Competent Group and was accompanied by uplift related to fault displacement and salt swelling. Conjugate listric faults formed during diapiric growth within the Fatha Formation and propagated upward into the Injana Formation and younger strata. Toward the northeast, faulting intensified and became more closely spaced, promoting greater deformation of the salt and leading to the formation of intersecting (conjugate) fault systems. This structural style aligns with analogue and numerical models [68], where horizontal shortening generates oppositely dipping fault pairs around vertical displacement zones such as rising diapirs. The distinctive curvature of these faults results from the interaction of two main forces: northeast-directed horizontal compression [71–73], accompanied by slight counterclockwise rotation, and vertical uplift from diapiric activity within the Fatha Formation. While they coincide spatially with deep-seated faults (Figure 5), their salt-controlled morphology warrants independent analysis. These faults do not appear at the surface, likely due to the presence of poorly consolidated clastic sediments and slow displacement rates along the fault planes. These conditions favored erosion and weathering, gradually obscuring and erasing surface fault expressions.

4.1. Salt Diapirism and Fault-Driven Deformation in the Buzurgan and Fauqi Fields

Salt diapirs are often positioned above inverted normal faults [74]. However, several studies conducted in Iran and Iraq [8,22,75] have not confirmed a direct correlation between salt deformation and deep-seated faults as the primary driving mechanism. These investigations, centered in areas closer to the collision zone, indicate that shortening and deformation are more pronounced in the upper stratigraphic layers than in the deeper ones, primarily due to contrasting rock competencies and the influence of salt movement. This dynamic has resulted in the displacement of salt diapirs or bulges away from the underlying deep faults. Consequently, some researchers have proposed that salt diapirism is largely governed by variations in overburden load or heterogeneities in overburden pressure, often originating from lateral variations in density or thickness [8,76]. Other suggested drivers include gravity-induced flow into structural lows [22], thermal gradients, buoyant forces, faulting [76], and tectonic pressurization of salt bodies [60]. Importantly, as emphasized by [77], salt deformation is not a one-mechanism phenomenon. Although salt is intrinsically buoyant and mobile, it can remain stable beneath thick overburden unless regional extension or shortening provides displacement loading. Such tectonic loading faults the overburden, generating zones of weakness that allow salt to mobilize. In this sense, faulting acts as a critical trigger, creating the structural conditions necessary for salt to respond to buoyant and gravitational forces.

The seismic data reveal the coexistence of salt pillows and salt diapirs, where pillows appear as low-relief uplifts adjacent to diapirs (Figure 5). Salt welds are also observed in places where migrating salt has evacuated, leaving direct contact between the overlying and underlying strata. These observed features indicate that pillows, diapirs, and welds represent different evolutionary stages of the same halokinetic system. Pillows likely formed under conditions of differential sedimentary

Preprints.org (www.preprints.org) | NOT PEER-REVIEWED | Posted: 1 October 2025 doi:10.20944/preprints202510.0031.v1

loading or localized thinning of the overburden, and their spatial association with diapirs suggests that some later evolved into diapirs as regional compression and basement fault reactivation provided the additional displacement loading required for vertical piercing. Together, the occurrence of pillows, diapirs, and welds underscores the progressive nature of halokinesis in the Missan oilfields and its strong mechanical linkage with basement-involved faults.

Although some of the observed faults might superficially resemble outer-arc extension features, their geometry and position argue against this interpretation. Outer-arc extension faults typically develop along the crest of anticlines due to bending stresses; however, in the study area, these faults occur on the eastern limb of the Fauqi fold rather than its crest (Figure 5). Furthermore, the elevated surface topography above the faulted zone (Figure 8) indicates a strong association with salt swelling and mobilization, rather than flexural extension of folded strata. These observations suggest that the faults are more plausibly linked to salt-related uplift and localized reactivation than to outer-arc extension.

An integrated surface–subsurface profile across the study area further demonstrates the strong linkage between surface morphology and subsurface structural deformation (Figure 8). The satellite imagery and topographic profile [78] reveal systematic elevation changes, with localized highs corresponding spatially to salt-related features identified in the seismic section. These elevated zones are not solely the product of erosional or depositional processes but instead reflect underlying structural controls exerted by salt mobility and deep-seated fault activity. The seismic section along the same transect highlights how basement-rooted faults and salt structures are mechanically coupled, producing disharmonic folding in the overburden that is mirrored in surface relief. This integration of surface and subsurface datasets provides independent support for the interpretation that salt–fault interactions play a first-order role in shaping both subsurface architecture and surface geomorphology in the Missan oilfields. Beyond structural interpretation, this integrated surface–subsurface analysis carries significant exploration and operational implications. The spatial correspondence between surface relief and subsurface deformation provides a cost-effective reconnaissance tool for predicting salt-related structures in unexplored areas. In hydrocarbon exploration, recognizing these surface expressions enhances the ability to delineate potential migration pathways and trapping geometries. Furthermore, integrating topographic signals with seismic data improves pre-drilling risk assessment by identifying structurally complex zones prone to abnormal pressures, salt-induced drilling hazards, or compartmentalized reservoirs. This is particularly critical in the Missan oilfields, where such challenges are recurrent and have direct implications for drilling safety and reservoir management. Thus, the combined analysis of topographic and seismic datasets not only clarifies the structural framework but also contributes directly to safer and more efficient exploration and field development strategies in salt-influenced tectonic provinces.

Preprints.org (www.preprints.org) | NOT PEER-REVIEWED | Posted: 1 October 2025 doi:10.20944/preprints202510.0031.v1

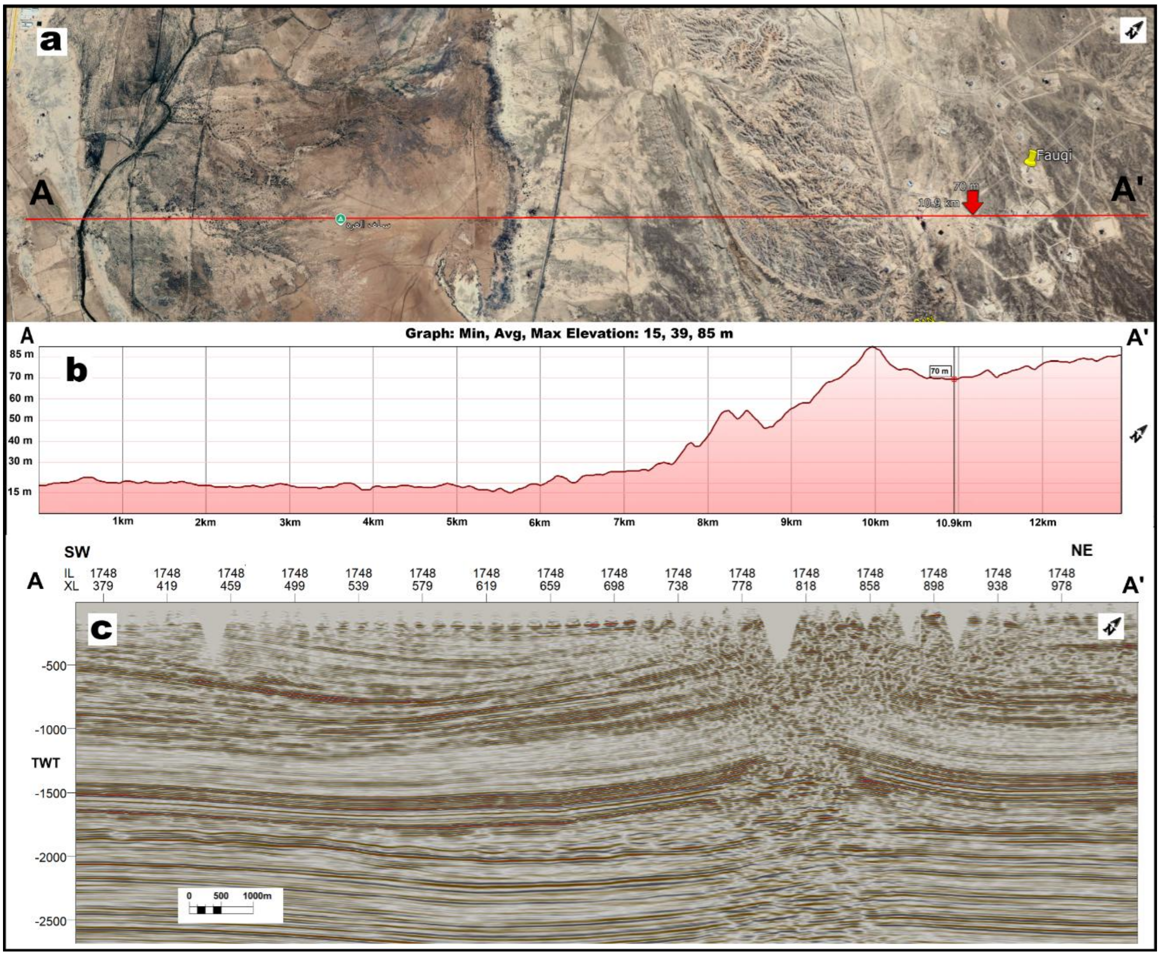

Figure 8. Integrated surface–subsurface profile along section A–A′ from west of the Buzurgan oilfield to the Fauqi oilfield. (a) Satellite imagery from Google Earth Pro (modified) showing the trace of the profile (red line) across the study area. (b) Topographic profile derived from Google Earth elevation data along the same trace, illustrating elevation changes with minimum, average, and maximum values indicated. (c) Corresponding seismic section oriented SW–NE, revealing subsurface structural configuration. The surface topography clearly corresponds with salt-related deformation, which is spatially linked to deep-seated fault systems.

The observed evolution of salt structures is consistent with the established stages of diapirism described by [60] and [77]. Initial broad pillows, observed in the study area as low-relief uplifts adjacent to diapirs (Figure 5), correspond to passive diapirism, driven by differential sedimentary loading. Subsequent intensification under regional compression reflects reactive diapirism, where regional shortening provided additional displacement loading. Finally, localized vertical piercing and strong upward propagation in stages (Figure 9e–f) are characteristic of the active phase, in which buoyancy and tectonic stresses jointly drove salt rise.

doi:10.20944/preprints202510.0031.v1

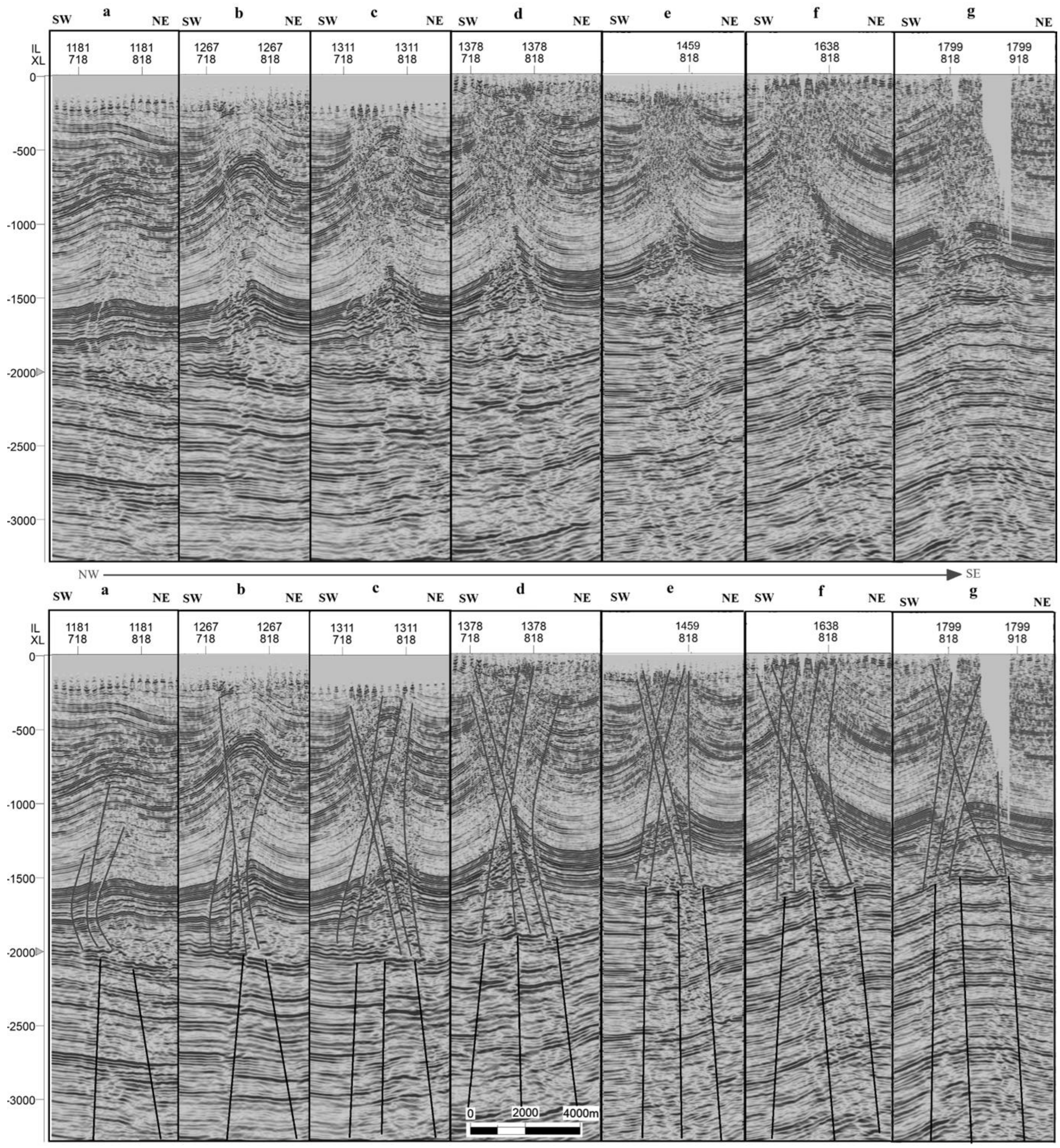

Figure 9. (a) Non-interpreted and (b) interpreted parallel inline seismic sections trending southeast, perpendicular to the fold axis on the western limb of the Fauqi fold. The sequence from (a) to (g) illustrates the progressive deformation and diapir development of the Mobile Group, coinciding with the weakening of the overburden by deep-seated faults and driven by deep fault zone activity (location shown in Figure 2).

The timing of salt piercing through the overburden remains a topic of debate among researchers [8,79,80]. Diapirism in the present study area appears to be less intense than in the further northeast zones, closer to the collisional margin. Therefore, we suggest that the examined sections represent an optimal setting for investigating the initiation of diapirism, providing valuable insight into the early stages of salt mobilization, particularly as this region lies at the interface between the folded and Mesopotamian zones. Figure 9 displays a sequence of parallel inline seismic sections progressing southeastward, perpendicular to the fold axis on the western limb of the Fauqi anticline. These images chronicle the progressive development of diapirism and faulting across seven stages (a–g). Stage (a) reveals the first rupture or piercement within the overburden, which coincides with the weakening of the upper layers by deep-seated faults. These ruptures appear as oblique listric faults, formed by the combined influence of horizontal compression and vertical uplift associated with salt swelling. As the process advances, the listric faults intensify, and deeper faults exhibit stronger deformation. During stages (b–d), faulting propagates through the upper layers, accompanied by the emergence of cross-conjugate fault patterns due to bidirectional salt movement. In stages (e) and (f), the fault intensity within the mobile and upper layers increases, coinciding with significant deformation of the deeper faults. Finally, in stage (g), the intensity of the listric faults diminishes, likely reflecting a reduction in activity and deformation of the deeper structures. This staged evolution illustrates the transition from passive pillows to active diapirism, providing a model applicable to regions with comparable tectonic and depositional settings.

4.2. Tectonic Evolution and Structural Development of the Buzurgan and Fauqi Anticlines

Building on [62]—who showed that pre-existing normal faults in rifted basins are commonly inverted to thrusts during fold-and-thrust belt development and that salt/shale horizons act as effective décollements decoupling structural levels—a kinematic model is proposed for the Buzurgan and Fauqi anticlines. The model, constrained by regional tectonic history and seismic evidence along inline 1748, synthesizes key observations (Figures 5 and 9) within the established geodynamic framework. Figure 10 presents this conceptual kinematic evolution and the successive stages inferred from the data.

(a) Rifting Phase: During the Triassic, regional extension associated with the opening of the Neo-Tethys Ocean initiated rifting, forming normal faults within the basement and overlying strata.

(b) Post-Rift Passive Margin: Following rifting, horizontal strata accumulated in a passive margin setting from the Late Triassic through much of the Cenozoic, during which the Neo-Tethys Ocean remained open in the area, forming a prolonged passive margin.

(c) Onset of shortening (Late Miocene): Convergence across the Arabia–Eurasia margin initiated folding and reverse reactivation of older normal faults; syn-kinematic growth strata developed adjacent to active structures.

(d) Progressive folding and faulting (Pliocene–Quaternary): Shortening intensified; reverse faults propagated upward, piercing the Mobile Group (salt-bearing Fatha units), with continued syn-kinematic deposition.

(e) Decoupling and structural disharmony: A primary, low-angle décollement formed within the Mobile Group, promoting mechanical decoupling between incompetent and competent packages and fostering the development of listric and conjugate fault systems.

(f) Present-day 3D architecture: Significant shortening is concentrated within the Mobile and Incompetent Groups; a major detachment occurs along R4 with localized detachment along R2, explaining observed disharmonic folding and local syncline-over-anticline geometries.

Growth strata above R2 (Figures 5 and 10f) display more pronounced folding and shortening than those below, reflecting their younger age, lower compaction, and greater susceptibility to deformation. In contrast, strata below R2 have been deformed over a longer timespan but are more lithified, showing reduced folding. Similarly, layers above R4 exhibit greater folding than those below, with R4 representing the principal décollement surface where total shortening reached approximately 3.5 km [81] and R2 acting as a secondary, localized décollement.

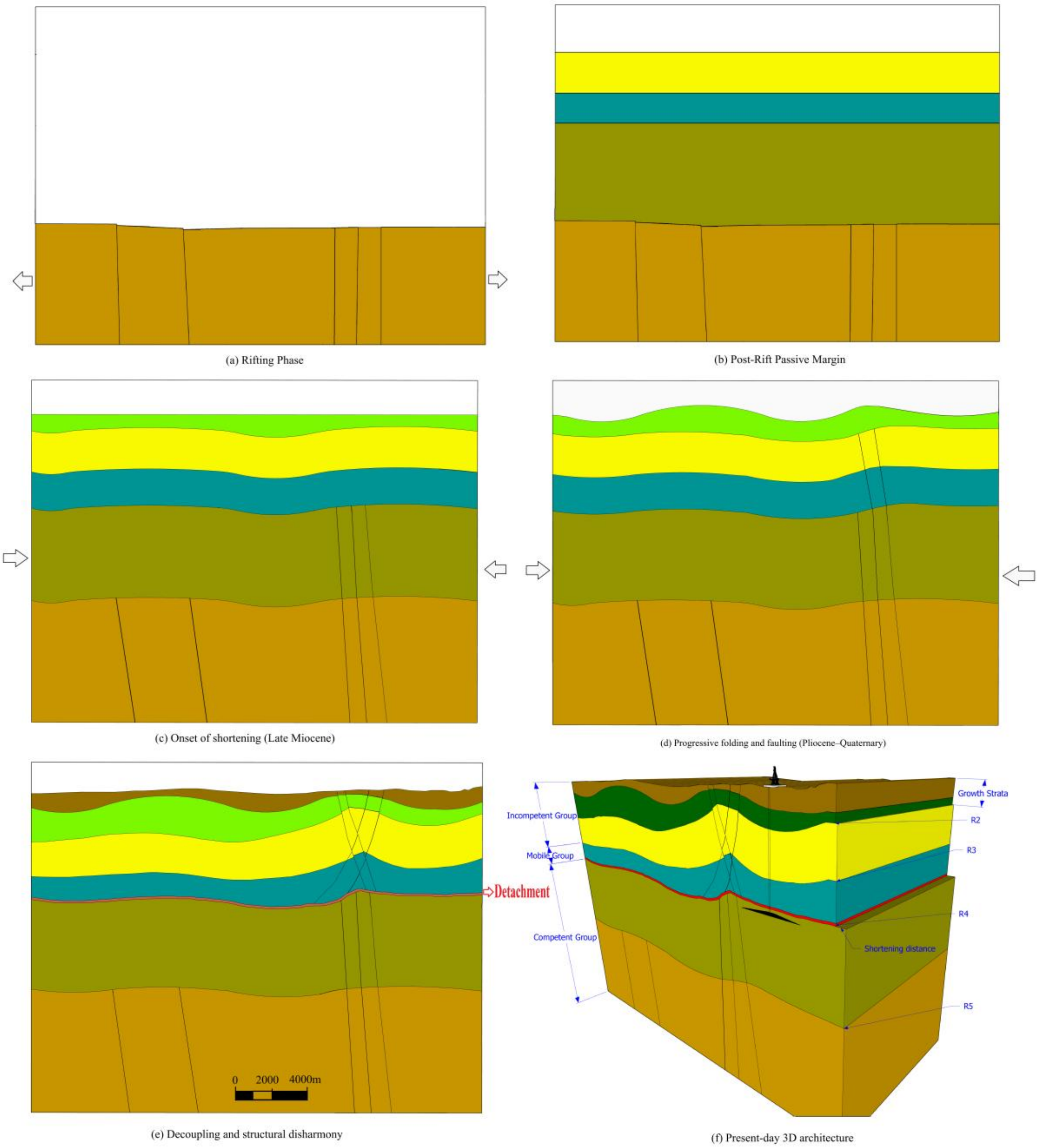

Figure 10. Integrated seismic–tectonic kinematic model of the Buzurgan and Fauqi anticlines, constructed from seismic interpretation (inline 1748) and the regional tectonic history derived from previous studies. The stages (a–f) depict the structural evolution from Triassic rifting to the present-day configuration, highlighting the roles of fault reactivation, salt-related décollement, and progressive folding.

4.3. Structural Evolution of the Dezful Embayment

The Dezful Embayment contains numerous north–south and northeast–southwest trending structures, widely interpreted as expressions of reactivated deep-seated basement faults [10,44,82–84]. Within the study area, the northwest–southeast–trending structures are interpreted to be more strongly controlled by basement architecture and the rheological layering of the cover than by Alpine compression alone [85]. Alpine deformation, acting on this inherited fabric, played a key role in localizing anticlines [46]. Seismic sections (Figures 5 and 11) reveal a spatial coincidence between deep-seated faults and anticlinal culminations, growth strata above R2, and mechanical decoupling across the Fatha evaporites, collectively indicating basement fault reactivation, block uplift, and fault-related folding in the study area.

 doi:10.20944/preprints202510.0031.v1

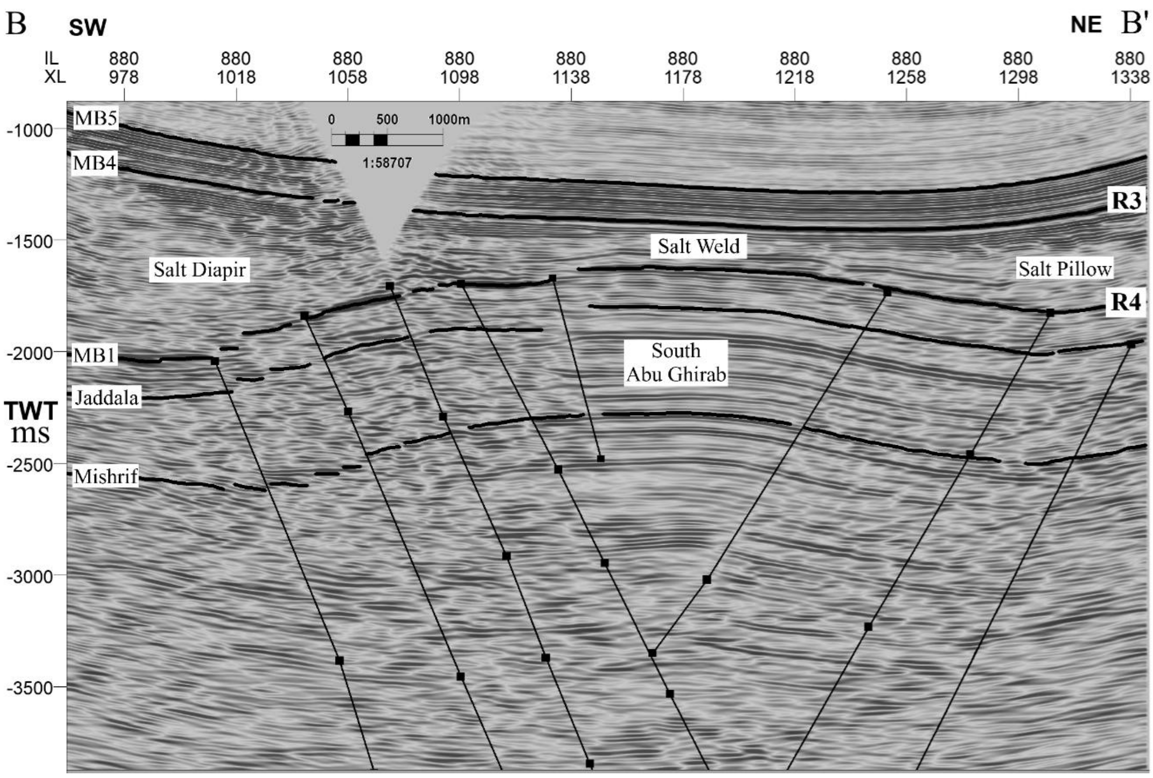

Figure 11. Inline seismic section B–B′ across the Abu Ghirab anticline (location in Figure 2), illustrating intense faulting and fracturing associated with salt deformation within the Mobile Group. The section displays features such as a salt diapir, salt weld, and salt pillow, along with deep-seated basement faults that significantly influenced the structural evolution and hydrocarbon migration in the field.

4.4. Deep-Seated Fault Dynamics

The ZFF delineates the frontal boundary of the ZFTB, separating it from the Mesopotamian Foredeep and Persian Gulf [40,86]. Seismic activity in the ZFTB is mainly concentrated along major arcuate basement faults termed "master blind thrusts," of which the ZFF is considered one [42,87,88].

Many studies interpret the ZFF as a reverse (thrust) fault formed during the Arabian–Eurasian collision [42,89,90]. However, others argue—based on seismic evidence—that it originated as a normal fault during the Late Triassic opening of the Neo-Tethys Ocean, later reactivated in reverse during the Pliocene to the present [40,46,86,91–93]. [46] further suggested that Late Cretaceous extensional events influenced parts of the fault zone. This view is consistent with observations from the Buzurgan field, where Cretaceous formations (e.g., Mishrif Formation) are not affected by faulting. In contrast, in the Fauqi and Abu Ghirab fields, the ZFF clearly offsets Cretaceous units (Figures 5 and 11). This contrast indicates either localized Cretaceous extension or spatial variability in fault reactivation. Seismic data indicate two distinct fault behaviors. Some faults terminate in deeper stratigraphic levels and appear inactive. In contrast, other faults extend upward into younger strata and are associated with reactivation, particularly within the Mobile Group.

[40] proposed that the ZFF in Iran, along with the Badra-Amarah Fault, Makhul Fault, Sinjar Fault (Iraq), and Abdul-Aziz Fault (Syria), constitutes a segmented fault system divided by transverse faults. These segments are collectively referred to as the ZFF, a naming convention adopted here, as the fault in this region is part of the Badra-Amarah system. However, the exact trace and lateral extent of the ZFF remain uncertain in several areas.

Folding geometry and growth-strata relationships provide further temporal constraints. In the Buzurgan field (Figure 5), deformation styles remained relatively consistent until the Late Miocene, when variations in growth-strata thickness began to appear. In contrast, the Faqi and Abu Ghirab fields exhibit significant deformation in the overlying layers, attributable to fault reactivation coupled with salt mobilization. Collectively, these observations suggest that folding and reverse reactivation

 doi:10.20944/preprints202510.0031.v1

along the ZFF were most pronounced during the Pliocene, following the deposition of the Injana Formation in the Late Miocene.

4.5. Impact of Deep-Seated Faults on Hydrocarbon Migration and Reservoir Development

Faults played a crucial role in the migration and accumulation of hydrocarbons, particularly in regions with significant stratigraphic separation between source rocks and reservoir units. The effectiveness of fault-assisted migration depended on the magnitude of displacement activity, rate, and timing relative to hydrocarbon generation and expulsion [94,95]. In faulted basins, faults often serve as primary conduits for vertical migration. Their efficiency was influenced by activity intensity, fault geometry, and the formation of secondary structures such as fractures, which could enhance or impede fluid movement [96,97].

The Abu Ghirab, Fauqi, and Buzurgan oilfields in southeastern Iraq are adjacent fields, yet they exhibit distinct hydrocarbon distribution patterns due to variations in fault dynamics and sealing formations.

1. Abu Ghirab Oilfield

Hydrocarbon production was primarily sourced from the Kirkuk (Asmari) Formation, which was heavily influenced by active faulting. Significant structural deformation occurred, including the development of numerous secondary faults and fractures (Figure 11), establishing effective vertical migration pathways from deeper units into the Kirkuk reservoir. Therefore, the Mishrif Formation demonstrated limited productive capacity. The Fatha Formation served as a robust regional seal, preventing further vertical migration of hydrocarbons.

2. Fauqi Oilfield

Hydrocarbons were extracted from both the Kirkuk and Mishrif Formations. Although fault activity was less intense than in Abu Ghirab, it remained sufficient to facilitate migration into both reservoirs. The observed hydrocarbon distribution reflected a balance between moderate fault activity and the sealing integrity of surrounding strata.

3. Buzurgan Oilfield

Hydrocarbon production was concentrated in the Mishrif Formation, with limited vertical migration to the Kirkuk Formation. Faults in the Buzurgan field appeared less prominent. They were characterized by subdued expression in seismic profiles (Figure 5), with minimal vertical displacement and limited lateral continuity, thereby reducing their effectiveness as migration pathways. As a result, hydrocarbons remained confined to the deeper Mishrif reservoir.

In summary, variations in fault activity and associated deformation exerted a primary control on hydrocarbon migration across the three fields. In Abu Ghirab, intense faulting and pervasive fracturing created efficient vertical pathways, allowing hydrocarbons to bypass deeper reservoirs and accumulate in the Kirkuk Formation. Meanwhile, the Fatha Formation—comprising largely evaporites, including thick layers of salt—served as a robust regional seal. Although its salt-rich intervals were involved in deformation and interacted with faults, their inherently ductile and sealing nature prevented hydrocarbons from migrating into shallower stratigraphic levels. In Fauqi, moderate fault activity supported migration into both the Mishrif and Kirkuk reservoirs, reflecting a balance between fault-assisted connectivity and sealing capacity. In contrast, Faults in the Buzurgan field are subdued in seismic expression and largely inactive, which reduces their effectiveness as migration pathways and confines hydrocarbons largely to the Mishrif reservoir. Collectively, these differences highlight how fault dynamics, deformation timing, and the sealing capacity of the Fatha Formation jointly governed the spatial distribution of hydrocarbons in the study area.

4.6. Operational and Drilling Implications of Salt Deformation

The structural impact of salt has direct implications for drilling operations in the Missan area. Thick, deformed evaporitic intervals within the Fatha Formation redistribute stress within mechanically weaker layers—particularly shale—thereby elevating formation pressures. As shown in Table 1, the onset of salt in unit MB4 coincides with a sharp increase in the pressure coefficient—

 doi:10.20944/preprints202510.0031.v1

from approximately 1.04 in the overlying interval to ~2.2—which persists through MB2 owing to the continuity of salt layers. By contrast, MB1, where salt is absent, shows a rapid return to near-normal pressure conditions. These anomalies highlight the structural complexity induced by salt deformation and directly contribute to operational challenges, such as mud loss, stuck pipe, and cementing difficulties, particularly across intervals with abrupt pressure transitions.

From an operational standpoint, recognizing these structural controls is crucial for accurate pre-drilling hazard prediction and effective well design. In structurally complex zones, such as Abu Ghirab and Fauqi, where salt deformation is most pronounced, proactive design strategies and continuous pressure monitoring are essential. By contrast, the Buzurgan field generally exhibits lower-intensity salt deformation and a correspondingly lower pressure risk, although localized complications may still arise. Integrating the structural model into drilling engineering helps reduce errors in casing-setting depth selection, lowers the risk of shoe instability and unexpected kicks, and ultimately enhances both safety and efficiency.

5. Conclusions

The deep-seated faults in the Missan region exhibit a complex evolutionary history of activity and reactivation. Some faults terminate within Triassic or Jurassic strata and appear inactive, whereas others—belonging to the broader Badra-Amarah system of the ZFF—extend upward into the mobile group. This pattern indicates an early phase of normal faulting, later overprinted by reverse reactivation that began in the Pliocene, following the deposition of the Late Miocene Injana Formation.

The structural evolution of the Missan fields reveals marked spatial contrasts. In the Buzurgan field, limited fault reactivation resulted in relatively uniform folding until the Late Miocene, with growth-strata thickness controlled mainly by syn-folding deposition and compaction contrasts rather than faulting. In contrast, the Fauqi and Abu Ghirab fields experienced listric faulting, amplified by salt swelling, which produced structural disharmony expressed by synclines over anticlines and deformed growth strata. Evidence also suggests localized Late Cretaceous extension, particularly in Fauqi and Abu Ghirab, where faults propagated beyond the Cretaceous strata. In contrast, the Mishrif Formation remained largely unaffected in Buzurgan, reflecting the spatial selectivity of extensional forces.

Clusters of closely spaced faults and intense deformation promoted significant salt mobilization, enhancing the complexity of listric geometries and forming conjugate fault patterns. The vertical alignment of salt structures with deep-seated basement faults highlights a strong mechanical linkage between fault reactivation and halokinesis.

Regionally, these deep-seated faults beneath the Buzurgan, Fauqi, and Abu Ghirab anticlines correlate with broader structural architecture, reflecting Alpine compressional stresses from the Arabia–Eurasia collision. Basement reactivation and block uplift under compression drove the fault-related folding observed across the area.

Importantly, fault activity exerted a primary control on hydrocarbon migration and accumulation. In Abu Ghirab, high fault activity—reflected by elevated fault density and cumulative throw—enabled efficient vertical migration into shallower reservoirs. In Fauqi, moderate fault activity allowed hydrocarbons to charge both shallow and deep reservoirs. In Buzurgan, limited fault activity largely restricted hydrocarbons to deeper intervals. These contrasts underscore the combined influence of fault connectivity, deformation timing, and seal integrity (e.g., the Fatha) on hydrocarbon distribution, highlighting fault reactivation and seal efficiency as key controls on reservoir development in the Missan oilfields.

Beyond subsurface insights, the study also reveals a strong correspondence between surface morphology and subsurface deformation. Morphologic highs and lineaments identified in satellite and topographic data spatially coincide with salt-related deformation and basement-rooted faults imaged in seismic sections. This surface–subsurface correspondence not only validates the structural interpretations but also provides practical exploration value by offering a cost-effective reconnaissance tool to predict subsurface complexity, reduce exploration risk, and guide optimal well placement in salt-influenced tectonic provinces.

Author Contributions: Conceptualization, Hayder Yousif and Xuri Huang; methodology, Hayder Yousif; software, Hayder Yousif; validation, Xuri Huang and Guanyu Zhang; formal analysis, Hayder Yousif; investigation, Hayder Yousif; resources, Xuri Huang; data curation, Hayder Yousif; writing—original draft preparation, Hayder Yousif; writing—review and editing, Xuri Huang and Guanyu Zhang; visualization, Hayder Yousif and Guanyu Zhang; supervision, Xuri Huang; project administration, Xuri Huang; funding acquisition, Xuri Huang.

Funding: This work was partially supported by the National Natural Science Foundation of China (42241206, U24B2022).

Acknowledgments: The authors would like to express their sincere gratitude to the Iraqi Ministry of Oil and Missan Oil Company for providing access to seismic and well-log data, which made this research possible. We also extend our appreciation to Southwest Petroleum University for its continuous support.

Conflicts of Interest: The authors declare that they have no known competing financial interests or personal relationships that could have appeared to influence the work reported in this paper.

References

1. Wang, R.; Tong, Y.; Zhang, Y.; Wu, C.; Zhu, Y.; Wang, G.; Wu, J.; Yang, P.; Tan, C. Demystifying Dynamic Evolution of Fault System and Its Controls on Karsted Reservoirs by Multi-Technology Integration. In Proceedings of the Day 1 Mon, March 13, 2023; SPE, March 13, 2023.
2. Markou, N.; Papanastasiou, P. 3D Geomechanical Finite Element Analysis for a Deepwater Faulted Reservoir in the Eastern Mediterranean. *Rock Mech Rock Eng* **2024**, doi:10.1007/s00603-024-03806-9.
3. Oppo, D.; Jackson, C.A.L.; Maselli, V. Early Extensional Salt Tectonics Controls Deep-Water Sediment Dispersal. *Geol Soc Am Bull* **2024**, doi:10.1130/B37786.1.
4. Gasda, S.E.; Keilegavlen, E.; Sandve, H.; Berge, R.; Pettersson, P.; Krumscheid, S. Practical Field-Scale Simulation Approaches for Quantification of Fault-Related Leakage under Uncertainty. In Proceedings of the 16th International Conference on Greenhouse Gas Control Technologies, GHGT-16; Lyon, France, 2022.
5. Zhu, D.; Wang, S.; Zheng, J.; Wang, Y.; Shi, C.; Zhao, R.; Ding, C.; Zang, X.; Meng, Y.; Han, B.; et al. Faults Internal Structure and Its Influence on Hydrocarbon Migration. *Academic Journal of Environment & Earth Science* **2024**, *6*, 26–36, doi:10.25236/ajee.2024.060404.
6. Xu, B.; Miocic, J.M.; Cheng, Y.; Xu, L.; Ma, S.; Sun, W.; Chu, Y.; Wu, Z. Fault Controls on Hydrocarbon Migration—An Example from the Southwestern Pearl River Mouth Basin. *Applied Sciences (Switzerland)* **2024**, *14*, doi:10.3390/app14051712.
7. O'Brien, C.A.E. Tectonic Problems of the Oilfield Belt of Southwest Iran. *In: 18th International Geological Congress* **1950**, *Proceeding*, 45–58.
8. O'Brien, C.A.E. Salt Diapirism in South Persia. *Geologie en Mijnbouw 19* **1957**, 357–367.
9. Stöcklin, J. Salt Deposits of the Middle East. *The Geological Society of America* **1968**, 157–182, doi:10.1130/SPE88-p157.
10. Sherkati, S.; Letouzey, J. Variation of Structural Style and Basin Evolution in the Central Zagros (Izeh Zone and Dezful Embayment), Iran. *Mar Pet Geol* **2004**, *21*, 535–554, doi:10.1016/j.marpetgeo.2004.01.007.
11. Taghikhani, H.; Yassaghi, A.; Madanipour, S.; Najafi, M. Salt Tectonics along the High Zagros Fault in Iran, Faulting through Welded Salt Walls. *J Asian Earth Sci* **2024**, *259*, doi:10.1016/j.jseaes.2023.105928.
12. Arian, M.; Noroozpour, H. Tectonic Geomorphology of Iran's Salt Structures. *Open Journal of Geology* **2015**, *05*, 61–72, doi:10.4236/ojg.2015.52006.
13. Hassanpour, J.; Muñoz, J.A.; Yassaghi, A.; Ferrer, O.; Jahani, S.; Santolaria, P.; SeyedAli, S.M. Impact of Salt Layers Interaction on the Salt Flow Kinematics and Diapirism in the Eastern Persian Gulf, Iran: Constraints from Seismic Interpretation, Sequential Restoration, and Physical Modelling. *Tectonophysics* **2021**, *811*, doi:10.1016/j.tecto.2021.228887.

14. Hassanpour, J.; Yassaghi, A.; Muñoz, J.A.; Jahani, S. Salt Tectonics in a Double Salt-Source Layer Setting (Eastern Persian Gulf, Iran): Insights from Interpretation of Seismic Profiles and Sequential Cross-Section Restoration. *Basin Research* **2020**, *33*, 159–185, doi:10.1111/bre.12459.
15. Shamszadeh, A.; Sarkarinejad, K.; Ferrer, O.; Mukherjee, S.; Seraj, M. Interaction of Inherited Structures and Contractional Deformation in the South Dezful Embayment: Insights from the Gachsaran Oilfield, SW Iran. *Mar Pet Geol* **2022**, *145*, doi:10.1016/j.marpetgeo.2022.105871.
16. Najafi, M.; Lajmorak, S. Contractional Salt-Tectonic System in the South Dezful Embayment, Zagros. *J Struct Geol* **2020**, *141*, doi:10.1016/j.jsg.2020.104204.
17. Alavi, M. Tectonics of the Zagros Orogenic Belt of Iran: New Data and Interpretations. *Tectonophysics* **1994**, *229*, 211–238, doi:10.1016/0040-1951(94)90030-2.
18. Soleimani, M.; Mann, J.; Shahsavani, H.; Shahbazi, A. Structural Interpretation of East Dezful Embayment in Zagros Fold-Thrust Belt by Seismic Sections.; Society of Exploration Geophysicists, September 17 2012; pp. 1–4.
19. Molinaro, M.; Leturmy, P.; Guezou, J.C.; Frizon de Lamotte, D.; Eshraghi, S.A. The Structure and Kinematics of the Southeastern Zagros Fold-Thrust Belt, Iran: From Thin-Skinned to Thick-Skinned Tectonics. *Tectonics* **2005**, *24*, 1–19, doi:10.1029/2004TC001633.
20. Derikvand, B.; Alavi, S.A.; Fard, I.A.; Jalali, L. Changing in Fold Geometry from Faulted Detachment Fold to Fault-Bend Fold, a Case Study: The Zeloi Anticline in the Dezful Embayment, Southwest of Iran. *J Pet Sci Eng* **2019**, *173*, 381–401, doi:10.1016/j.petrol.2018.10.033.
21. Derikvand, B.; Alavi, S.A.; Fard, I.A.; Hajialibeigi, H. Folding Style of the Dezful Embayment of Zagros Belt: Signatures of Detachment Horizons, Deep-Rooted Faulting and Syn-Deformation Deposition. *Mar Pet Geol* **2018**, *91*, 501–518, doi:10.1016/j.marpetgeo.2018.01.030.
22. Sherkati, S.; Molinaro, M.; Frizon de Lamotte, D.; Letouzey, J. Detachment Folding in the Central and Eastern Zagros Fold-Belt (Iran): Salt Mobility, Multiple Detachments and Late Basement Control. *J Struct Geol* **2005**, *27*, 1680–1696, doi:10.1016/j.jsg.2005.05.010.
23. Abdollahie Fard, I.; Sepehr, M.; Sherkati, S. Neogene Salt in SW Iran and Its Interaction with Zagros Folding. *Geol Mag* **2011**, *148*, 854–867, doi:10.1017/S0016756811000343.
24. Al-hlaichi, S.K.; Al-Mahdawi, F.H.M.; Ali, J.A. Drilling Optimization by Using Advanced Drilling Techniques in Buzurgan Oil Field. *Iraqi Journal of Chemical and Petroleum Engineering* **2023**, *24*, 53–64, doi:10.31699/ijcpe.2023.2.6.
25. Alhusseini, A.K.; Hamd-Allah, S. Estimation of Initial Oil in Place for Buzurgan Oil Field by Using Volumetric Method and Reservoir Simulation Method. *Iraqi Geological Journal* **2022**, *55*, 106–120, doi:10.46717/igj.55.2C.9ms-2022-08-22.
26. Abdulrazzaq, T.; Togun, H.; Haider, D.; Ali, M.; Hamadi, S. Determining of Reservoir Fluids Properties Using PVTP Simulation Software- a Case Study of Buzurgan Oilfield. In Proceedings of the E3S Web of Conferences; EDP Sciences, November 11 2021; Vol. 321.
27. Mohammed, M.M.; Salih, H.M.; Mnaty, K.H. 3D Reservoir Modeling of Buzurgan Oil Field, Southern Iraq. *Iraqi Journal of Science* **2022**, *63*, 596–607, doi:10.24996/ijs.2022.63.2.16.
28. Aldarraji, M.Q.; Almayahi, A.Z. Seismic Structure Study of Buzurgan Oil Field, Southern Iraq. *Iraqi Journal of Science* **2019**, *60*, 610–623, doi:10.24996/ijs.2019.60.3.19.
29. Duffy, O.; Hudec, M.; Peel, F.; Apps, G.; Bump, A.; Moscardelli, L.; Dooley, T.; Bhattacharya, S.; Wisian, K.; Shuster, M. The Role of Salt Tectonics in the Energy Transition: An Overview and Future Challenges. *Tektonika* **2023**, *1*, doi:10.55575/tektonika2023.1.1.11.
30. Koyi, H.A.; Ghasemi, A.; Hessami, K.; Dietl, C. The Mechanical Relationship between Strike-Slip Faults and Salt Diapirs in the Zagros Fold–Thrust Belt. *J Geol Soc London* **2008**, *165*, 1031–1044, doi:10.1144/0016-76492007-142.
31. Sharland, P.R.; Archer, R.; Casey, D.M.; Davies, R.B.; Hall, S.H.; Heward, A.P.; Horbury, A.D.; Simmons, M.D. *Arabian Plate Sequence Stratigraphy*; GeoArabia Special P2.; Gulf Petrolink, 2001; ISBN 9901-03-08-9.
32. Sadooni, F.N.; Alsharhan, A.S. Stratigraphy, Lithofacies Distribution, and Petroleum Potential of the Triassic Strata of the Northern Arabian Plate. *Am Assoc Pet Geol Bull* **2004**, *88*, 515–538, doi:10.1306/12030303067.

33. Basit, A.; Umar, M.; Jamil, M.; Qasim, M. Facies Analysis and Depositional Framework of Late Permian-Jurassic Sedimentary Successions, Western Salt Range, Pakistan: Implications for Sequence Stratigraphic Trends and Paleogeography of the Neo-Tethys Sea. *Kuwait Journal of Science* **2022**, doi:10.48129/kjs.16575.
34. Agard, P.; Omrani, J.; Jolivet, L.; Whitechurch, H.; Vrielynck, B.; Spakman, W.; Monie, P.; Meyer, B.; Wortel, R. Zagros Orogeny: A Subduction-Dominated Process. *Geol Mag* **2011**, *148*, 692–725, doi:10.1017/S001675681100046X.
35. Navabpour, P.; Angelier, J.; Barrier, E. Mesozoic Extensional Brittle Tectonics of the Arabian Passive Margin, Inverted in the Zagros Collision (Iran, Interior Fars). *Geological Society, London, Special Publications* **2010**, *330*, 65–96, doi:10.1144/SP330.5.
36. Abdollahie Fard, I.; Sherkati, S.; McClay, K.; Haq, B.U. Tectono-Sedimentary Evolution of the Iranian Zagros in a Global Context and Its Impact on Petroleum Habitats. In; 2019; pp. 17–28.
37. Glennie, K.W. Cretaceous Tectonic Evolution of Arabia's Eastern Plate Margin: A Tale of Two Oceans. In *Middle East Models of Jurassic/Cretaceous Carbonate System*; Alsharhan, A.S., Scott, R.W., Eds.; SEPM (Society for Sedimentary Geology), 2000; Vol. 69, pp. 9–20.
38. Al-Juboury, A.I.; McCann, T. The Middle Miocene Fatha (Lower Fars) Formation, Iraq. *GeoArabia* **2008**, *13*, 141–174, doi:10.2113/geoarabia1303141.
39. Aqrawi, A.A.M.; Goff, J.; Horbury, A.D.; Sadooni, F. *The Petroleum Geology of Iraq*; 1st ed.; The Petroleum Geology of Iraq, 2010; ISBN 978-0-901360-36-8.
40. Al-Kaabi, M.; Abdulnaby, W. Seismotectonics of the Zagros Foredeep Fault (ZFF), NE Arabian Plate. *Arabian Journal of Geosciences* **2022**, *15*, doi:10.1007/s12517-022-10448-0.
41. Homke, S.; Vergés, J.; Garcés, M.; Emami, H.; Karpuz, R. Magnetostratigraphy of Miocene-Pliocene Zagros Foreland Deposits in the Front of the Push-e Kush Arc (Lurestan Province, Iran). *Earth Planet Sci Lett* **2004**, *225*, 397–410, doi:10.1016/j.epsl.2004.07.002.
42. Berberian, M. Master "Blind" Thrust Faults Hidden under the Zagros Folds: Active Basement Tectonics and Surface Morphotectonics. *Tectonophysics* **1995**, *241*, 193–224, doi:10.1016/0040-1951(94)00185-C.
43. Talbot, C.J.; Alavi, M. The Past of a Future Syntaxis across the Zagros. *Geol Soc Spec Publ* **1996**, *100*, 89–109, doi:10.1144/GSL.SP.1996.100.01.08.
44. Abdollahie Fard, I.; Braathen, A.; Mokhtari, M.; Alavi, S.A. Interaction of the Zagros Fold-Thrust Belt and the Arabian-Type, Deep-Seated Folds in the Abadan Plain and the Dezful Embayment, SW Iran. *Petroleum Geoscience* **2006**, *12*, 347–362, doi:10.1144/1354-079305-706.
45. Joudaki, M.; Faghih, A.; Mukherjee, S.; Seraj, M.; Soleimany, B. Structural Style & Kinematic Analysis of Deformation in the Northern Dezful Embayment, Zagros Fold-Thrust Belt, SW Iran. *Mar Pet Geol* **2024**, *170*, doi:10.1016/j.marpetgeo.2024.107122.
46. Jassim, S.Z.; Goff, J.C. *Geology of Iraq*; Dolin, Prague and Moravian Museum: Brno, 2006; ISBN 8070282878.
47. Shawkat, M.G.; Tucker, M.E. Stromatolites and Sabkha Cycles from the Lower Fars Formation (Miocene) of Iraq. *Geologische Rundschau* **1978**, *67*, 1–14, doi:10.1007/BF01803253.
48. Gill, W.D.; Ala, M.A. Sedimentology of Gachsaran Formation (Lower Pars Series), Southwest Iran'. *Am Assoc Pet Geol Bull* **1972**, *56*, 1965–1974, doi:10.1306/819A41A0-16C5-11D7-8645000102C1865D.
49. Gemmer, L.; Ings, S.J.; Medvedev, S.; Beaumont, C. Salt Tectonics Driven by Differential Sediment Loading: Stability Analysis and Finite-element Experiments. *Basin Research* **2004**, *16*, 199–218, doi:10.1111/j.1365-2117.2004.00229.x.
50. Zucker, E.; Gvirtzman, Z.; Steinberg, J.; Enzel, Y. Salt Tectonics in the Eastern Mediterranean Sea: Where a Giant Delta Meets a Salt Giant. *Geology* **2020**, *48*, 134–138, doi:10.1130/G47031.1.
51. Rowan, M.G.; Urai, J.L.; Carl Fiduk, J.; Kukla, P.A. Deformation of Intrasalt Competent Layers in Different Modes of Salt Tectonics. *Solid Earth* **2019**, *10*, 987–1013, doi:10.5194/se-10-987-2019.
52. Bellen, R.C. van; Dunnington, H. V.; Wetzel, R.; Morton, D.M. *- Iraq.- Lexique Stratigraphique International*; Paris: Centre National de la Recherche Scientifique: Iraq, 1959; Vol. III, Asie, Fascicule;
53. Sayyab, A.; Kureshy, A.A. The Benthonic Foraminifera of the Lower Fars Formation (Lower Miocene) from Shathatha, Karbala, Iraq. *college of science, Baghdad* **1967**, 139–149.
54. James, A.D.; Wynd, B. Stratigraphic Nomenclature of Iranian Oil Consortium Agreement Area. *Am. Assoc. Petroleum Geologists Bull* **1965**, *49*, 2182–2245.

55. Mahmoodabadi, R.M. Facies Analysis, Sedimentary Environments and Correlative Sequence Stratigraphy of Gachsaran Formation in SW Iran. *Carbonates Evaporites* **2020**, *35*, doi:10.1007/s13146-020-00555-y.
56. Mehrgini, B.; Memarian, H.; Dusseault, M.B.; Ghavidel, A.; Heydarizadeh, M. Geomechanical Characteristics of Common Reservoir Caprock in Iran (Gachsaran Formation), Experimental and Statistical Analysis. *J Nat Gas Sci Eng* **2016**, *34*, 898–907, doi:10.1016/j.jngse.2016.07.058.
57. Rezaee, P.; Salari, Sh. Petrography and Mineralogy of Gachsaran Formation in West of Bandar-e-Abbas, Kuh-e-Namaki Khamir Section, South of Iran. *Journal of Fundamental and Applied Sciences* **2016**, *8*, 956, doi:10.4314/jfas.v8i2s.151.
58. Bulant, P.; Klimeš, L. Comparison of VSP and Sonic-Log Data in Nonvertical Wells in a Heterogeneous Structure. *Geophysics* **2008**, *73*, doi:10.1190/1.2907243.
59. Fouad, S.F.A. TECTONIC MAP OF IRAQ, SCALE 1: 1000 000, 3rd EDITION, 2012. *Iraqi Bulletin of Geology and Mining* **2015**, *11*, 1–7.
60. Hudec, M.R.; Jackson, M.P.A. Terra Infirma: Understanding Salt Tectonics. *Earth Sci Rev* **2007**, *82*, 1–28, doi:10.1016/j.earscirev.2007.01.001.
61. Vatandoust, M.; Faghih, A.; Burberry, C.M.; Shafiei, G. Structural Style and Kinematic Analysis of Folding in the Southern Dezful Embayment Oilfields, SW Iran. *J Struct Geol* **2020**, *134*, doi:10.1016/j.jsg.2020.103989.
62. Jackson, J.A. Reactivation of Basement Faults and Crustal Shortening in Orogenic Belts. *Nature* **1980**, *283*, 343–346, doi:10.1038/283343a0.
63. Sepehr, M.; Cosgrove, J.; Moieni, M. The Impact of Cover Rock Rheology on the Style of Folding in the Zagros Fold-Thrust Belt. *Tectonophysics* **2006**, *427*, 265–281, doi:10.1016/j.tecto.2006.05.021.
64. Sherkati, S.; Letouzey, J.; De Lamotte, D.F. Central Zagros Fold-Thrust Belt (Iran): New Insights from Seismic Data, Field Observation, and Sandbox Modeling. *Tectonics* **2006**, *25*, doi:10.1029/2004TC001766.
65. Riahi, Z.T.; Soleimany, B.; Sarkarinejad, K.; Faghih, A.; Payrovian, G.R. Deciphering Multi-Phase Inversion Tectonics in the Southern Dezful Embayment: Insights from the Rag-e-Sefid Oilfield, SW Iran. *Int Geol Rev* **2024**, *66*, 680–701, doi:10.1080/00206814.2023.2207190.
66. Price, R.A. The Southeastern Canadian Cordillera: Thrust Faulting, Tectonic Wedging, and Delamination of the Lithosphere*. *J Struct Geol* **1986**, *3*, doi:https://doi.org/10.1016/0191-8141(86)90046-5.
67. Amos, C.B.; Burbank, D.W.; Nobes, D.C.; Read, S.A.L. Geomorphic Constraints on Listric Thrust Faulting: Implications for Active Deformation in the Mackenzie Basin, South Island, New Zealand. *J Geophys Res Solid Earth* **2007**, *112*, doi:10.1029/2006JB004291.
68. Ferrill, D.A.; Smart, K.J.; Cawood, A.J.; Morris, A.P. The Fold-Thrust Belt Stress Cycle: Superposition of Normal, Strike-Slip, and Thrust Faulting Deformation Regimes. *J Struct Geol* **2021**, *148*, doi:10.1016/j.jsg.2021.104362.
69. Patalakha, Y.I. The Problem of Listric Faults. *Int Geol Rev* **1986**, *28*, 1416–1422, doi:10.1080/00206818609466376.
70. Williams, G. The Geometry of Listric Normal Faults and Deformation in Their Hanging Walls. *J Struct Geol* **1987**, *9*, 789–795, doi:10.1016/0191-8141(87)90080-0.
71. Vernant, P.; Chéry, J. Mechanical Modelling of Oblique Convergence in the Zagros, Iran. *Geophys J Int* **2006**, *165*, 991–1002, doi:10.1111/j.1365-246X.2006.02900.x.
72. Albino, I.; Cavazza, W.; Zattin, M.; Okay, A.I.; Adamia, S.; Sadradze, N. Far-Field Tectonic Effects of the Arabia–Eurasia Collision and the Inception of the North Anatolian Fault System. *Geol Mag* **2014**, *151*, 372–379, doi:10.1017/S0016756813000952.
73. Reilinger, R.; McClusky, S.; Vernant, P.; Lawrence, S.; Ergintav, S.; Cakmak, R.; Ozener, H.; Kadirov, F.; Guliev, I.; Stepanyan, R.; et al. GPS Constraints on Continental Deformation in the Africa-Arabia-Eurasia Continental Collision Zone and Implications for the Dynamics of Plate Interactions. *J Geophys Res Solid Earth* **2006**, *111*, doi:10.1029/2005JB004051.
74. Del Ventisette, C.; Montanari, D.; Bonini, M.; Sani, F. Salt Diapirism during Basin Inversion: Inferences from Analogue Mode Lling. *Rendiconti della Società Geologica Italiana, Nuova Serie* **2005**, *1*, 1–2.
75. Dunnington, H. V. Salt-Tectonic Features of Northern Iraq. In *Saline Deposits: A Symposium based on Papers from the International Conference on Saline Deposits, Houston, Texas, 1962*; Mattox, R.B., Holser, W.T., Ode, H.,

McIntire, W.L., Short, N.M., Taylor, R.E., Van Siclen, D.C., Eds.; The Geological Society of America, 1968; pp. 183–223.
76. Suppe, John. *Principles of Structural Geology*; 2nd ed.; Prentice-Hall, 2005; ISBN 0137105002,9780137105007.
77. Jackson, M.P.A.; Hudec, M.R. *Salt Tectonics*; Cambridge University Press, 2017; ISBN 9781139003988.
78. Google Earth Pro Satellite Imagery and Elevation Profile of the Missan Oilfields, Iraq Available online: https://earth.google.com/web/@32.14390314,47.56520578,55333.21211648a,0d,35y,15.5083h,0.7065t,-0r/data=CgRCAggBOgMKATBCAggASg0I____________ARAA?utm_source=earth7&utm_campaign=vine&hl=en (accessed on 16 August 2025).
79. Smith, D.A.; Reeve, F.A.E. Salt Piercement in Shallow Gulf Coast Salt Structures. *The American Association of Petroleum Geologists Bulletin V* **1970**, *54*, 1271–1289, doi:10.1306/5d25cbb9-16c1-11d7-8645000102c1865d.
80. Yang, K.; Qi, J.; Shen, F.; Sun, T.; Duan, Z.; Cui, M.; Li, P.; Lv, J. Formation Mechanism of Salt Piercement Structures in a Compressive Environment: An Example from the Kuqa Depression, Western China. *J Struct Geol* **2024**, *178*, 105005, doi:10.1016/j.jsg.2023.105005.
81. Ou, C.H.; Chen, W.; Li, C.C.; Zhou, W.J. Structural Geometrical Analysis and Simulation of Decollement Growth Folds in Piedmont Fauqi Anticline of Zagros Mountains, Iraq. *Sci China Earth Sci* **2016**, *59*, 1885–1898, doi:10.1007/s11430-016-5332-6.
82. Sepehr, M.; Cosgrove, J.W. Structural Framework of the Zagros Fold-Thrust Belt, Iran. *Mar Pet Geol* **2004**, *21*, 829–843, doi:10.1016/j.marpetgeo.2003.07.006.
83. Farahzadi, E.; Alavi, S.A.; Sherkati, S.; Ghassemi, M.R. Variation of Subsidence in the Dezful Embayment, SW Iran: Influence of Reactivated Basement Structures. *Arabian Journal of Geosciences* **2019**, *12*, doi:10.1007/s12517-019-4758-5.
84. Alavi, M. Structures of the Zagros Fold-Thrust Belt in Iran. *Am J Sci* **2007**, *307*, 1064–1095, doi:10.2475/09.2007.02.
85. Al Naqib, K.M. *Geology of the Arabian Peninsula Southwestern Iraq*; United States Government Printing Office: Washington, 1967;
86. Abdulnaby, W.; Motaghi, K.; Shabanian, E.; Mahdi, H.; Al-Shukri, H.; Gök, R. Crustal Structure of the Mesopotamian Plain, East of Iraq. *Tectonics* **2020**, *39*, doi:10.1029/2020TC006225.
87. Karasözen, E.; Nissen, E.; Bergman, E.A.; Ghods, A. Seismotectonics of the Zagros (Iran) From Orogen-Wide, Calibrated Earthquake Relocations. *J Geophys Res Solid Earth* **2019**, *124*, 9109–9129, doi:10.1029/2019JB017336.
88. Alsinawi, S.A. Seismicity. In *Geology of Iraq*; Jassim, S., Goff, J., Eds.; Dolin, Prague and Moravian Museum: Brno, 2006; pp. 91–101.
89. Mobasher, K. Kinematic Significance of Fold- and Fault-Related Fracture Systems in the Zagros Mountains, Southern Iran. *Tectonophysics* **2007**, *451*, 156–169, doi:10.1016/j.tecto.2007.11.060.
90. Jackson, M.P.A.; Talbot, C.J. External Shapes, Strain Rates, and Dynamics of Salt Structures. *Geol Soc Am Bull* **1986**, *97*, 305–323, doi:10.1130/0016-7606(1986)97<305:ESSRAD>2.0.CO;2.
91. Abdulnaby, W. Structural Geology and Neotectonics of Iraq, Northwest Zagros. In *Developments in Structural Geology and Tectonics*; Ali Farzipour Saein, Ed.; Elsevier, 2019; Vol. 3, pp. 53–73 ISBN 9780128150481.
92. Darweesh, H.A.; Obed, A.Z.M.; Albadran, B.N. Structural Study of Basins Configuration in Mesopotamian Area. *International Journal of Engineering and Applied Sciences (IJEAS)* **2017**, *4*, 54–58.
93. Abdulnaby, W.; Mandeel, M.; Al-Mohmed, R.; Mahdi, H.; Mahdi, M.; Mahdi, H.H. Seismotectonics of Badra-Amarah Fault, Iraq-Iran Border. *IOSR Journal of Applied Geology and Geophysics* **2016**, *4*, 27–33, doi:10.9790/0990-0403022733.
94. Jiang, Y.; Liu, H.; Song, G.; Wang, Y.; Liu, J.; Zhao, K.; LÜ, X. Differential Hydrocarbon Enrichment and Its Main Controlling Factors in Depressions of the Bohai Bay. *ACTA GEOLOGICA SINICA* **2017**, *91*, 1855–1872, doi:10.1111/1755-6724.13415.
95. Jiang, Y.; Liu, P.; Song, G. Late Cenozoic Faulting Activities and Their Influence upon Hydrocarbon Accumulations in the Neogene in Bohai Bay Basin. *Oil & Gas Geology* **2015**, *36*, doi:10.11743/ogg20150401.
96. Hindle, A.D. Petroleum Migration Pathways and Charge: A Three-Dimensional Model. *The American Association of Petroleum Geologists* **1997**, *81*, 1451–1481.

 doi:10.20944/preprints202510.0031.v1

97. Jiang, Y.; Kai, Z.; Liu, J.; LÜ, X. A Quantitative Method for Evaluating the Transporting Capacity of Oil-Source Faults in Shallow Formation of Oil-Rich Sags. *Acta Geologica Sinica - English Edition* **2018**, *92*, 1678–1679, doi:10.1111/1755-6724.13663.